Journal of Computational Physics 277 (2014) 48–71

Contents lists available at ScienceDirect

Journal of Computational Physics

www.elsevier.com/locate/jcp

Second order convex splitting schemes for periodic nonlocal Cahn–Hilliard and Allen–Cahn equations

Zhen Guan [a,*], John S. Lowengrub [a], Cheng Wang [b,c], Steven M. Wise [d]

[a] Mathematics Department, University of California, Irvine, CA 92697, USA
[b] Mathematics Department, University of Massachusetts Dartmouth, North Dartmouth, MA 02747, USA
[c] School of Mathematical Sciences, Soochow University, Suzhou, Jiangsu 215006, PR China
[d] Mathematics Department, University of Tennessee, Knoxville, TN 37996, USA

ARTICLE INFO

Article history:
Received 10 May 2013
Received in revised form 18 July 2014
Accepted 2 August 2014
Available online 8 August 2014

Keywords:
Nonlocal Cahn–Hilliard equation
Energy stability
Unique solvability
Multigrid

ABSTRACT

We devise second-order accurate, unconditionally uniquely solvable and unconditionally energy stable schemes for the nonlocal Cahn–Hilliard (nCH) and nonlocal Allen–Cahn (nAC) equations for a large class of interaction kernels. We present numerical evidence that both schemes are convergent. We solve the nonlinear equations resulting from discretization using an efficient nonlinear multigrid method and demonstrate the performance of our algorithms by simulating nucleation and crystal growth for several different choices of interaction kernels.

1. Introduction

In this paper our primary goal is to develop second order accurate schemes for a family of integro-partial-differential equations:

$$\partial_t \phi = \nabla \cdot \big(M(\phi)\nabla w\big) \quad \text{in } (0,T]\times\Omega, \tag{1}$$

and

$$\partial_t \phi = -M(\phi) w \quad \text{in } (0,T]\times\Omega, \tag{2}$$

with the initial condition

$$\phi(0,x) = \phi_0(x) \quad \text{in } \Omega, \tag{3}$$

where Ω is a rectangular domain in $\mathbb{R}^n$, $M(\phi) > 0$ is the mobility, $w = \delta_\phi E$ is the chemical potential (δ_ϕ is the variational derivative) and E is a nonlocal interaction energy. While we take ϕ to be Ω-periodic in the sequel, the results regarding the non-local part of the system can be extended to homogeneous boundary conditions with minor modifications by calculating the convolution integrals below as proposed for example in [13]. The nonlocal energy E is assumed to have the form

$$E = \int_\Omega \left(F(\phi) - \frac{1}{2}\int_\Omega J(\mathbf{x}-\mathbf{y})\phi(\mathbf{x})\phi(\mathbf{y})d\mathbf{y}\right)d\mathbf{x}, \tag{4}$$

* Corresponding author.
E-mail addresses: guanz2@math.uci.edu (Z. Guan), lowengrb@math.uci.edu (J.S. Lowengrub), cwang1@umassd.edu (C. Wang), swise@math.utk.edu (S.M. Wise).

http://dx.doi.org/10.1016/j.jcp.2014.08.001
0021-9991/

where the interaction kernel $J:\mathbb{R}^n \to \mathbb{R}$ is also Ω-periodic and satisfies $J(-\mathbf{x}) = J(\mathbf{x})$. F is the (local) homogeneous energy density and is typically nonlinear. Defining the circular, or periodic, convolution[1] for smooth Ω-periodic function ϕ and J as

$$(J * \phi)(\mathbf{x}) := \int_\Omega J(\mathbf{y})\,\phi(\mathbf{x}-\mathbf{y})d\mathbf{y} = \int_\Omega J(\mathbf{x}-\mathbf{y})\,\phi(\mathbf{y})d\mathbf{y}, \tag{5}$$

the chemical potential w may be expressed as

$$w := \delta_\phi E = F'(\phi) - J * \phi. \tag{6}$$

We refer to Eqs. (1) and (2) as nonlocal Cahn–Hilliard (nCH) and nonlocal Allen–Cahn (nAC) equations respectively. These are nonlocal versions of the classical Cahn–Hilliard (CH) and Allen–Cahn (AC) equations, the CH equation being the conserved gradient flow, and the AC being the non-conserved gradient flow of the (local) free energy [17,2,18]

$$E_{loc}(\phi) = \int_\Omega \left(G(\phi) + \frac{\epsilon^2}{2}|\nabla\phi|^2 \right) d\mathbf{x}. \tag{7}$$

A direct connection between the local and nonlocal energies can be seen as follows. Introducing the inner product notation on Ω, $(f,g)_{L^2(\Omega)} := \int_\Omega f(\mathbf{x})g(\mathbf{x})\,d\mathbf{x}$, the energy in Eq. (4) can be written as

$$E(\phi) = \big(F(\phi),1\big)_{L^2(\Omega)} - \frac{1}{2}(\phi, J*\phi)_{L^2(\Omega)}. \tag{8}$$

The energy $E_{loc}(\phi)$ is obtained by approximating the nonlocal convolution term in E [5,16,27,39,55]. Specifically, one takes the approximation $J*\phi \approx J_0\phi + \frac{1}{2}J_2\Delta\phi$ where $J_0 := \int_\Omega J(\mathbf{x})d\mathbf{x}$ and $J_2 := \int_\Omega J(\mathbf{x})|\mathbf{x}|^2\,d\mathbf{x}$ (the second moment of J). Under the assumption of periodic boundary conditions,

$$\frac{1}{2}(\phi, J*\phi)_{L^2(\Omega)} \approx \frac{1}{2}\left(\phi, J_0\phi + \frac{1}{2}J_2\Delta\phi\right)_{L^2(\Omega)} = \frac{J_0}{2}(\phi,\phi)_{L^2(\Omega)} + \frac{J_2}{4}(\nabla\phi,\nabla\phi)_{L^2(\Omega)}. \tag{9}$$

Thus we can obtain E_{loc} with $G(\phi) := F(\phi) - \frac{J_0}{2}\phi^2$ and $\epsilon^2 = \frac{J_2}{2}$. By taking $w = \delta_\phi E_{loc}$ the corresponding classical CH and AC equations are

$$\partial_t\phi = \nabla\cdot\big(M(\phi)\nabla\big(G'(\phi) - \epsilon^2\Delta\phi\big)\big) \tag{10}$$

and

$$\partial_t\phi = -M(\phi)\big(G'(\phi) - \epsilon^2\Delta\phi\big). \tag{11}$$

In both the local and nonlocal models, energy is dissipated at the rates $-\|\sqrt{M}\nabla w\|^2_{L^2(\Omega)}$ (conserved dynamics) and $-\|\sqrt{M}w\|^2_{L^2(\Omega)}$ (non conserved dynamics) with w being the variational derivative of the appropriate energy (local/nonlocal).

Eqs. (1) and (2) have been widely used in many fields ranging from physics and materials science to biology, finance and image processing. In materials science, Eqs. (1), (2), (10), (11) and other closely related equations arise as mesoscopic models of interacting particle systems [5,39,22]. For example, in dynamic density functional theory (DDFT) [5,6], the interaction kernel $J = c^{(2)}(x,y|\phi_{ref})$ is the two-particle direct correlation function, ϕ represents the mesoscopic particle density and ϕ_{ref} is some reference density. See [27,46,47,50,51,55,29] for further details. In biology, J has been used to model interactions among cells and extracellular matrix [8,9,19,32]. In mathematical models of finance, J arises from an expectation taken with respect to a particular measure that is used in the model for option pricing [48]. In the case that Eq. (1) is used in the modeling for image segmentation, J is interpreted as the attracting force [30,31]. Theoretical studies of conservative, nonlocal equations Eq. (1) can be found in [12,14,15,20,31,33,34], while studies of non-conservative systems Eq. (2) can be found in [12,16,28].

A variety of methods have been developed to solve the equations like Eqs. (1) and (2). In general, spectral methods provide the most efficient algorithms to compute convolution-type nonlocal interactions via the fast Fourier transform (FFT), see for example [38,39]. Spectral methods have also been combined with the finite difference method (e.g. [3]). These approaches typically require periodic boundary conditions. Finite difference, finite volume and finite element methods offer more flexibility in terms of boundary conditions (e.g., see [13,23,24]), but these methods are not as efficient as spectral methods. Rational function approximations have also been used in the numerical simulation of convolution-type nonlocal interactions [49].

Regarding time discretization, most of schemes referenced above have used either explicit time stepping such as explicit Euler's method, the Adams–Bashforth method or semi-implicit algorithms such as the Crank–Nicolson method. While there

[1] The connection between the circular convolution and the classical whole-space convolution is briefly recounted in Appendix A.

has been some analysis of implicit methods (e.g. [1,52]), we are not aware of any results on uniquely solvable, unconditionally stable second order time discretizations.

In this paper we propose semi- and fully-discrete second order in time unconditionally energy stable schemes for the nCH and nAC equations under the assumption that $\Omega \subset \mathbb{R}^2$ is a rectangular domain and ϕ is periodic on Ω. Compared with previous results, our contribution focuses on efficient and robust high order time integration algorithms. We extend the second order time integration algorithm for the PFC presented in [41] to the nCH and nAC equations. Other high order convex splitting methods, such as the one described in [57], can also be extended to the nCH and nAC equations using a similar approach for the nonlocal terms as developed here. We demonstrate that our scheme is unconditionally energy stable and uniquely solvable, which is an extension of our previous results on the first order time integration algorithms [37]. Our approach provides a framework that can be combined with most existing spatial discretization methods, thus it has a wide range of applicability. The results in this paper can be extended straightforwardly to three dimensions.

This paper is organized in the following way. In Section 2 we present and analyze the semi-discrete schemes. In Section 3 the fully discrete schemes are proposed and their properties are discussed. In Section 4 we present numerical experiments which verify our theoretical results and demonstrate the capability of our schemes. Conclusions and future works are discussed in Section 5. Technical details are given in the appendices.

2. The semi-discrete second order schemes

Assume Ω is a rectangular domain in $\mathbb{R}^2$. Suppose that the interaction kernel J satisfies

(J1) $J = J_c - J_e$, where J_c, J_e are non-negative, Ω-periodic, and smooth functions.
(J2) $J_c(-\mathbf{x}) = J_c(\mathbf{x})$ and $J_e(-\mathbf{x}) = J_e(\mathbf{x})$.
(J3) $\int_\Omega J(\mathbf{x})d\mathbf{x} > 0$.

The nonlocal part of energy (4) can be rewritten as

$$-\frac{1}{2}\int_\Omega\int_\Omega J(\mathbf{x}-\mathbf{y})\phi(\mathbf{x})\phi(\mathbf{y})d\mathbf{y}d\mathbf{x} = \frac{1}{4}\int_\Omega\int_\Omega J(\mathbf{x}-\mathbf{y})\big(\phi(\mathbf{x})-\phi(\mathbf{y})\big)^2 d\mathbf{y}d\mathbf{x} - \frac{1}{2}\int_\Omega \phi^2(\mathbf{y})\bigg(\int_\Omega J(\mathbf{x})d\mathbf{x}\bigg)d\mathbf{y}.$$

The convexity of the resulting functional depends on the sign of J. Condition (J1) will therefore be important for the development of our convex splitting schemes. Many interaction kernels admit such a splitting. The reader is referred to Eq. (65) in Section 4 for practical examples.

For the rest of the paper we assume that the local energy density $F(\phi)$ satisfies the following inequality:

$$F(\phi) \le a\phi^q + b, \tag{12}$$

where a, b are positive real constants and $q \ge 2$ is a positive integer, and

$$F(\phi) = F_c(\phi) - F_e(\phi), \tag{13}$$

where $F_c(\phi)$ and $F_e(\phi)$ are convex functions with respect to ϕ. An important example of a local energy density F that satisfies Eq. (12) and Eq. (13) is

$$F(\phi) = \frac{1}{4}\phi^4 + \frac{\gamma_c - \gamma_e}{\phi}^2, \tag{14}$$

where γ_c, $\gamma_e \ge 0$ are constants [26,35]. Here $F_c = \frac{1}{4}\phi^4 + \frac{\gamma_c}{2}\phi^2$ and $F_e = \frac{\gamma_e}{2}\phi^2$. Another important example is the regular solution model free energy [11,45]:

$$F(\phi) := \theta\big[\phi\log(\phi) + (1-\phi)\log(1-\phi)\big] - 2\theta_c\phi(1-\phi), \tag{15}$$

where θ and θ_c represent the absolute and critical temperatures, respectively. Due to the properties of the logarithm function, Eq. (15) needs to be regularized in order to fit in the framework of this paper, and the reader is referred to Appendix B for more details. An alternative, regularized form of logarithmic free energy can be found in [10].

Observe that the nCH equation (1) can be rewritten as

$$\partial_t\phi = \nabla\cdot\big(a(\phi)\nabla\phi\big) - \nabla\cdot\big(M(\phi)\nabla(J*\phi)\big), \tag{16}$$

where

$$a(\phi) = M(\phi)F''(\phi). \tag{17}$$

We refer to $a(\phi)$ as the diffusive mobility, or just the diffusivity. To make Eq. (1) positive diffusive (and non-degenerate), therefore, we require that

$$M(\phi)F''(\phi) > 0, \tag{18}$$

in which case $a(\phi) > 0$. Following [14,15] we will assume that Eq. (18) holds in the rest of the paper to make the problem well-posed.

To motivate the fully discrete scheme that will be presented later, we first provide semi-discrete versions of the scheme and briefly describe their properties. From Eq. (8), we have the following properties of the energy, which we state without proof:

Lemma 2.1. *If $F(\phi)$ satisfies Eqs. (12) and (13), the energy (8) can be written as the difference of convex functionals, i.e., $E = E_c - E_e$, where*

$$E_c(\phi) = \big(F_c(\phi), 1\big)_{L^2(\Omega)} + (J_c * 1)\|\phi\|^2_{L^2(\Omega)}, \tag{19}$$

$$E_e(\phi) = \big(F_e(\phi), 1\big)_{L^2(\Omega)} + (J_c * 1)\|\phi\|^2_{L^2(\Omega)} + \frac{1}{2}(\phi, J * \phi)_{L^2(\Omega)}. \tag{20}$$

The decomposition above is not unique but is the most useful for our purpose. We will use the following function in the rest of the paper:

$$\chi(\phi, \psi) := \begin{cases} \frac{F_c(\phi) - F_c(\psi)}{\phi - \psi}, & \phi \neq \psi, \\ F_c'(\phi), & \phi = \psi, \end{cases} \tag{21}$$

which we borrowed and modified from [45]. For Eq. (21) we have the following result:

Theorem 2.1. *Suppose $F_c(\phi)$ is convex, and define $\Gamma(\phi, \psi)$ as*

$$\partial_\phi \Gamma(\phi, \psi) = \chi(\phi, \psi). \tag{22}$$

Thus $\Gamma(\phi, \psi)$ is twice differentiable with respect to ϕ and $\Gamma(\phi, \psi)$ is convex with respect to ϕ for any fixed ψ.

The proof of this theorem is omitted for the sake of brevity.

A second-order (in time) convex splitting scheme for the nCH equation defined as Eq. (1) can be constructed as follows: given two Ω-periodic smooth functions ϕ^{k-1}, ϕ^k, find Ω-periodic smooth functions ϕ^{k+1}, $w^{k+\frac{1}{2}}$ such that

$$\phi^{k+1} - \phi^k = s\nabla \cdot \big(M(\hat{\phi}^{k+\frac{1}{2}})\nabla w^{k+\frac{1}{2}}\big), \tag{23}$$

$$w^{k+\frac{1}{2}} = \chi\big(\phi^k, \phi^{k+1}\big) + 2(J_c * 1)\phi^{k+\frac{1}{2}} - 2(J_c * 1)\hat{\phi}^{k+\frac{1}{2}} - \frac{3}{2}F_e'\big(\phi^k\big) + \frac{1}{2}F_e'\big(\phi^{k-1}\big) - J * \hat{\phi}^{k+\frac{1}{2}}, \tag{24}$$

where $s > 0$ is the time step and

$$\phi^{k+\frac{1}{2}} := \frac{1}{2}\big(\phi^{k+1} + \phi^k\big), \qquad \hat{\phi}^{k+\frac{1}{2}} := \frac{1}{2}\big(3\phi^k - \phi^{k-1}\big) \tag{25}$$

with $\phi^{-1} \equiv \phi^0$.

A second-order convex splitting scheme for the nAC equation defined as Eq. (2) can be constructed similarly. Given Ω-periodic smooth functions ϕ^{k-1}, ϕ^k, find Ω-periodic smooth functions ϕ^{k+1}, $w^{k+\frac{1}{2}}$ such that

$$\phi^{k+1} - \phi^k = -sM(\hat{\phi}^{k+\frac{1}{2}})w^{k+\frac{1}{2}}, \tag{26}$$

$$w^{k+\frac{1}{2}} = \chi\big(\phi^k, \phi^{k+1}\big) + 2(J_c * 1)\phi^{k+\frac{1}{2}} - 2(J_c * 1)\hat{\phi}^{k+\frac{1}{2}} - \frac{3}{2}F_e'\big(\phi^k\big) + \frac{1}{2}F_e'\big(\phi^{k-1}\big) - J * \hat{\phi}^{k+\frac{1}{2}}, \tag{27}$$

where $\phi^{-1} \equiv \phi^0$.

Notice that these two schemes respect the convex splitting of the energy E following Lemma 2.1 and that the full convolution is treated explicitly. The contribution to the chemical potential corresponding to the convex energy E_c is treated implicitly, using a secant approximation. The part corresponding to the concave part E_e is treated explicitly, via extrapolation. Under the assumption $F_e = \frac{\gamma}{2}\phi^2$, where γ is a nonnegative constant, we next define the pseudo energy:

$$\mathcal{E}\big(\phi^k, \phi^{k+1}\big) := E\big(\phi^{k+1}\big) + \frac{2(J_c * 1) + \gamma}{4}\big\|\phi^{k+1} - \phi^k\big\|^2_{L^2(\Omega)} + \frac{1}{4}\big(J * \big(\phi^{k+1} - \phi^k\big), \phi^{k+1} - \phi^k\big)_{L^2(\Omega)}, \tag{28}$$

where $E(\phi)$ is as defined in Eq. (8).

Remark 2.1. The forms of the second order schemes (23)–(24) and (26)–(27) will not guarantee the dissipation of the "physical" energy $E(\phi^k)$. To remedy this, we introduce the pseudo energy above, as in our previous works, e.g., [41]. Clearly, $E(\phi) = \mathcal{E}(\phi, \phi)$; in fact the pseudo energy is a consistent, second-order in time approximation of the physical energy. The precise form of the pseudo energy is motivated by an analysis of the discrete versions of the schemes (33)–(34) and

(35)–(36) in Section 3.3, and we have further assumed that $F_e = \frac{\gamma}{2}\phi^2$. More importantly, Theorem 2.2 below – whose proof is similar to the fully discrete analogue in Section 3.3 and is omitted for brevity – will show that our schemes do satisfy pseudo-energy stability, $\mathcal{E}(\phi^k, \phi^{k+1}) \le \mathcal{E}(\phi^{k-1}, \phi^k)$.

Remark 2.2. In the sequel we discuss properties of the energy stability under the assumption $F_e = \frac{\gamma}{2}\phi^2$, where γ is a nonnegative constant. However, numerical evidence indicates that (23)–(24), (26)–(27) and their fully discrete versions are unconditionally energy stable provided that F_e is a general convex function.

We can prove the following:

Theorem 2.2. *Assume ϕ^{k+1}, $w^{k+\frac{1}{2}}$ are Ω-periodic smooth solutions to the nCH scheme (23)–(24) and $F_e = \frac{\gamma}{2}\phi^2$ where γ is a nonnegative constant. Thus for any $k \ge 1$ and $s > 0$,*

$$\int_\Omega \phi^k \, d\mathbf{x} = \int_\Omega \phi^0 \, d\mathbf{x}, \tag{29}$$

and

$$\mathcal{E}\left(\phi^k, \phi^{k+1}\right) + s\left\|\nabla w^{k+\frac{1}{2}}\right\|^2_{L^2(\Omega)} \le \mathcal{E}\left(\phi^{k-1}, \phi^k\right). \tag{30}$$

In particular, the pseudo energy (28) is non-increasing, i.e., $\mathcal{E}(\phi^k, \phi^{k+1}) \le \mathcal{E}(\phi^{k-1}, \phi^k)$, and we say that the scheme is unconditionally pseudo energy stable.

Similarly, assume ϕ^{k+1}, $w^{k+\frac{1}{2}}$ are Ω-periodic smooth solutions to the nAC scheme (26)–(27). $F_e = \frac{\gamma}{2}\phi^2$ where γ is a nonnegative constant. For any $k \ge 1$ and $s > 0$,

$$\mathcal{E}\left(\phi^k, \phi^{k+1}\right) + s\left\|w^{k+\frac{1}{2}}\right\|^2_{L^2(\Omega)} \le \mathcal{E}\left(\phi^{k-1}, \phi^k\right), \tag{31}$$

and we say that the scheme is unconditionally pseudo energy stable.

Since the proofs of Theorem 2.2 and its discrete analogue in Section 3.3 are essentially the same, we skip the proof of the former for the sake of brevity.

Remark 2.3. Under the assumption that $F(\phi) = \frac{\phi^4}{4} + \frac{\gamma\phi^2}{2}$ where γ is a real constant, the convergence of fully discrete 2nd order scheme for nAC equation is proved in Section 5.6 of [36].

3. The second-order schemes and their properties

3.1. The fully discrete schemes

We now present the fully discrete second order energy stable schemes for nCH and nAC equations. We make extensive use of the spatially discrete operators, norms, function spaces, and summation-by-parts formulas described in Appendix C. The reader is directed there for full details. We begin by defining a fully discrete energy that is consistent with the continuous space energy (8). In particular, define the discrete energy $\overline{E} := \mathcal{C}_{m\times n} \to \mathbb{R}$ ($\mathcal{C}_{m\times n}$ denotes cell-centered functions, see Appendix C) to be

$$\overline{E}(\phi) := h^2\left(F(\phi)\|\mathbf{1}\right) - \frac{h^2}{2}\left(\phi\|[J\star\phi]\right), \tag{32}$$

where a cell-centered inner product $(\cdot\|\cdot)$ is defined in Eq. (84) and $[J\star\phi]$ is the discrete convolution defined in Eq. (99). Here $\mathbf{1}$ is a vector with all entries equal to 1.

A fully discrete second-order convex splitting scheme for the nCH equation can be constructed as follows: given $\phi^k \in \mathcal{C}_{m\times n}$ and periodic (defined in Eq. (92) in Appendix C), find ϕ^{k+1}, $w^{k+\frac{1}{2}} \in \mathcal{C}_{m\times n}$ periodic such that

$$\phi^{k+1} - \phi^k = sd_x\left(M\left(\frac{3}{2}A_x\phi^k - \frac{1}{2}A_x\phi^{k-1}\right)D_x w^{k+\frac{1}{2}}\right) + sd_y\left(M\left(\frac{3}{2}A_y\phi^k - \frac{1}{2}A_y\phi^{k-1}\right)D_y w^{k+\frac{1}{2}}\right), \tag{33}$$

$$w^{k+\frac{1}{2}} = \chi\left(\phi^k, \phi^{k+1}\right) + 2[J_c\star\mathbf{1}]\phi^{k+\frac{1}{2}} - \left(2[J_c\star\mathbf{1}]\right)\hat{\phi}^{k+\frac{1}{2}} - \frac{3}{2}F_e'\left(\phi^k\right) + \frac{1}{2}F_e'\left(\phi^{k-1}\right) - \left[J\star\hat{\phi}^{k+\frac{1}{2}}\right], \tag{34}$$

where $\phi^{-1} \equiv \phi^0$, and D_x, D_y, d_x, d_y denote discrete finite difference operators and A_x, A_y denote local averaging operators in the x- and y-direction. See Appendix C.

A fully second-order convex splitting scheme for the nAC equation can be constructed analogously: given $\phi^k \in \mathcal{C}_{m\times n}$ periodic, find ϕ^{k+1}, $w^{k+\frac{1}{2}} \in \mathcal{C}_{m\times n}$ periodic such that

$$\phi^{k+1} - \phi^k = -sM\big(\hat{\phi}^{k+\frac{1}{2}}\big)w^{k+\frac{1}{2}}, \tag{35}$$

$$w^{k+\frac{1}{2}} = \chi\big(\phi^k, \phi^{k+1}\big) + 2[J_c \star \mathbf{1}]\phi^{k+\frac{1}{2}} - \big(2[J_c \star \mathbf{1}]\big)\hat{\phi}^{k+\frac{1}{2}} - \frac{3}{2}F_e'\big(\phi^k\big) + \frac{1}{2}F_e'\big(\phi^{k-1}\big) - \big[J \star \hat{\phi}^{k+\frac{1}{2}}\big], \tag{36}$$

where $\phi^{-1} \equiv \phi^0$.

3.2. Unconditional unique solvability

Next we prove the unconditional unique solvability of these schemes using the methodology developed in [41].

Theorem 3.1. *The second order scheme (33)–(34) for the nCH equation is discretely mass conservative. Moreover, this scheme is uniquely solvable for any time step size $s > 0$. Similarly, the second order scheme (35)–(36) for the nAC equation is uniquely solvable for any time step size $s > 0$.*

Proof. Suppose that $\{\phi^{k+1},\ w^{k+\frac{1}{2}}\} \in [\mathcal{C}_{m\times n}]^2$ is a periodic solution pair to Eqs. (33) and (34). Then using the summation by parts formula and the periodic boundary conditions for $w^{k+\frac{1}{2}}$ gives

$$\begin{aligned}\big(\phi^{k+1} - \phi^k \big\| \mathbf{1}\big) &= s\big(d_x\big(M_{ew}^{\star} D_x w^{k+\frac{1}{2}}\big) + d_y\big(M_{ns}^{\star} D_y w^{k+\frac{1}{2}}\big)\big\|\mathbf{1}\big)\\ &= -s\big[M_{ew}^{\star} D_x w^{k+\frac{1}{2}} \big\| D_x\mathbf{1}\big]_{ew} - s\big[M_{ew}^{\star} D_y w^{k+\frac{1}{2}} \big\| D_y\mathbf{1}\big]_{ns} = 0,\end{aligned} \tag{37}$$

where $M_{ew}^{\star}$ and $M_{ns}^{\star}$ are the appropriate variables from scheme (33)–(34) defined as:

$$M_{ew}^{\star} := M\left(\frac{3}{2}A_x\phi^k - \frac{1}{2}A_x\phi^{k-1}\right) \tag{38}$$

and

$$M_{ns}^{\star} := M\left(\frac{3}{2}A_y\phi^k - \frac{1}{2}A_y\phi^{k-1}\right). \tag{39}$$

Here $[\cdot\|\cdot]_{ew}$ and $[\cdot\|\cdot]_{ew}$ denote edge centered inner products defined in Eqs (85) and (86). Hence $h^2(\phi^{k+1}\|\mathbf{1}) = h^2(\phi^k\|\mathbf{1})$. Introducing space H defined as

$$H = \big\{\phi \in \mathcal{C}_{m\times n} \ \big|\ (\phi\|\mathbf{1}) = 0 \text{ and } \phi \text{ is periodic}\big\},$$

and the reader is referred to Appendix C for details. Without loss of generality, we may suppose that the solution the periodic solution ϕ^k of scheme (33)–(34) is in H. Now, consider the following functional on H:

$$G_1(\phi) := \frac{h^2}{2s}\big(\phi - \phi^k \big\| \phi - \phi^k\big)_H + Q(\phi) + R(\phi), \tag{40}$$

where $(\cdot\|\cdot)_H$ denotes the mobility-weighted discrete bilinear form given by Eq. (104) in Appendix C,

$$Q(\phi) := h^2\big(\Gamma(\phi,\psi)\big\|\mathbf{1}\big) + [J_c \star \mathbf{1}]\|\phi\|_2^2 \tag{41}$$

and

$$R(\phi) := -h^2\left(\phi\left\|\big(2[J_c \star \mathbf{1}]\big)\hat{\phi}^{k+\frac{1}{2}} + \frac{3}{2}F_e'\big(\phi^k\big) - \frac{1}{2}F_e'\big(\phi^{k-1}\big) + \big[J \star \hat{\phi}^{k+\frac{1}{2}}\big]\right.\right) + h^2\big(\phi\big\|[J_c \star \mathbf{1}]\phi^k\big). \tag{42}$$

Define

$$W\big(\phi, \phi^k, \phi^{k-1}\big) = \delta_\phi\big[Q(\phi) + R(\phi)\big]. \tag{43}$$

By Theorem 2.1 the functional Q is strictly convex. This, together with the properties of the weighted bilinear form given in Appendix C, implies that $G_1(\phi)$ is strictly convex and coercive over H and its unique minimizer $\phi^* \in H$ satisfies

$$\begin{aligned}\phi^* - \phi^k = {} & sd_x\left(M\left(\frac{3}{2}A_x\phi^k - \frac{1}{2}A_x\phi^{k-1}\right)D_x W\big(\phi^*, \phi^k, \phi^{k-1}\big)\right)\\ & + sd_y\left(M\left(\frac{3}{2}A_y\phi^k - \frac{1}{2}A_y\phi^{k-1}\right)D_y W\big(\phi^*, \phi^k, \phi^{k-1}\big)\right),\end{aligned} \tag{44}$$

which is exactly Eq. (33) by identifying $\phi^{k+1} = \phi^*$ and $w^{k+\frac{1}{2}} = W(\phi^{k+1}, \phi^k, \phi^{k-1})$. Thus minimizing the strictly convex functional $G_1(\phi)$ over the affine space H, is the same as solving the second-order convex splitting scheme (33)–(34). This completes the proof for the nCH scheme.

Regarding the solvability of (35)–(36), consider the functional

$$G_2(\phi) := \frac{1}{2sM(\hat{\phi}^{k+\frac{1}{2}})}\left\|\phi-\phi^k\right\|_2^2 + Q(\phi) + R(\phi). \tag{45}$$

Then it can be shown that $G_2(\phi)$ is strictly convex and coercive over the set of admissible functions

$$\mathcal{A} = \{\phi \in \mathcal{C}_{m\times n} \mid \phi \text{ is periodic}\}, \tag{46}$$

and its unique minimizer $\phi^* \in \mathcal{A}$ satisfies the discrete Euler–Lagrange equation

$$\delta_\phi G_2(\phi^*) = \frac{\phi^*-\phi^k}{sM(\hat{\phi}^{k+\frac{1}{2}})} + w^{k+\frac{1}{2}} = 0, \tag{47}$$

which is equivalent to Eq. (35) by taking $\phi^{k+1}=\phi^*$. Thus minimizing the strictly convex functional $G_2(\phi)$ over the set of admissible functions $\mathcal{A}$ is the same as solving the second-order convex splitting scheme (35)–(36). This completes the proof for the nAC scheme. □

3.3. Unconditional energy stability

We now prove results concerning the unconditional energy stability of the schemes. As in the semi-discrete case, under the assumption $F_e = \frac{\gamma}{2}\phi^2$ where γ is a nonnegative constant, we define the discrete pseudo energy as

$$\mathcal{F}(\phi^k,\phi^{k+1}) := \bar{E}(\phi^{k+1}) + \frac{2[J_c\star\mathbf{1}]+\gamma}{4}\left\|\phi^{k+1}-\phi^k\right\|_2^2 + \frac{h^2}{4}\left([J\star(\phi^{k+1}-\phi^k)]\|\phi^{k+1}-\phi^k\right), \tag{48}$$

where $\bar{E}(\phi)$ is as defined in Eq. (32).

Lemma 3.1. *For any periodic functions $\phi, \psi \in \mathcal{C}_{m\times n}$*

$$\bar{E}(\phi) \le \mathcal{F}(\psi,\phi). \tag{49}$$

Proof. By Proposition C.5 in Appendix C and the properties of J, we can show that

$$\frac{2[J_c\star\mathbf{1}]+\gamma}{4}\left\|\phi^{k+1}-\phi^k\right\|_2^2 + \frac{h^2}{4}\left([J\star(\phi^{k+1}-\phi^k)]\|\phi^{k+1}-\phi^k\right) \ge 0, \tag{50}$$

which proves the claim. □

Theorem 3.2. *Set $F_e = \frac{\gamma}{2}\phi^2$ where γ is a nonnegative constant. Suppose that $\{\phi^{k+1},\ w^{k+\frac{1}{2}}\} \in [\mathcal{C}_{m\times n}]^2$ is a periodic solution pair to (33)–(34). Then we have*

$$\mathcal{F}(\phi^k,\phi^{k+1}) + s\left\|\nabla_h w^{k+\frac{1}{2}}\right\|_M^2 + \mathcal{R}(\phi^{k-1},\phi^k,\phi^{k+1}) = \mathcal{F}(\phi^{k-1},\phi^k), \tag{51}$$

for any $s>0$, where

$$\begin{aligned}\mathcal{R}(\phi^{k-1},\phi^k,\phi^{k+1}) = {}& \frac{2[J_c\star\mathbf{1}]+\gamma}{4}\left\|\phi^{k+1}-2\phi^k+\phi^{k-1}\right\|_2^2 \\ & + \frac{h^2}{4}\left([J\star(\phi^{k+1}-2\phi^k+\phi^{k-1})]\|\phi^{k+1}-2\phi^k+\phi^{k-1}\right)\end{aligned} \tag{52}$$

and

$$\begin{aligned}\left\|\nabla_h w^{k+\frac{1}{2}}\right\|_M^2 := {}& h^2\left[\left(M\left(\frac{3}{2}A_x\phi^k-\frac{1}{2}A_x\phi^{k-1}\right)D_x w^{k+\frac{1}{2}}\middle\| D_x w^{k+\frac{1}{2}}\right)\right]_{ew} \\ & + h^2\left[\left(M\left(\frac{3}{2}A_y\phi^k-\frac{1}{2}A_y\phi^{k-1}\right)D_y w^{k+\frac{1}{2}}\middle\| D_y w^{k+\frac{1}{2}}\right)\right]_{ns}.\end{aligned} \tag{53}$$

Similarly, if $\{\phi^{k+1},\ w^{k+\frac{1}{2}}\} \in [\mathcal{C}_{m\times n}]^2$ is a periodic solution pair to the scheme (35)–(36), we have

$$\mathcal{F}(\phi^k,\phi^{k+1}) + s\left(M(\hat{\phi}^{k+\frac{1}{2}})w^{k+\frac{1}{2}}\|w^{k+\frac{1}{2}}\right) + \mathcal{R}(\phi^{k-1},\phi^k,\phi^{k+1}) = \mathcal{F}(\phi^{k-1},\phi^k), \tag{54}$$

for any $s>0$. The remainder term, $\mathcal{R}(\phi^{k-1},\phi^k,\phi^{k+1})$, is non-negative. This implies that the pseudo energy is non-increasing, i.e., *$\mathcal{F}(\phi^k,\phi^{k+1}) \le \mathcal{F}(\phi^{k-1},\phi^k)$, for both (33)–(34) and (35)–(36).*

Proof. We first note that the following identities hold:

$$h^2\big(\chi(\phi^k,\phi^{k+1})\|\phi^{k+1}-\phi^k\big)=h^2\big(F_c(\phi^{k+1})\|\mathbf{1}\big)-h^2\big(F_c(\phi^k)\|\mathbf{1}\big), \tag{55}$$

$$h^2\big(\phi^{k+\frac{1}{2}}\|\phi^{k+1}-\phi^k\big)=\frac{1}{2}\|\phi^{k+1}\|_2^2-\frac{1}{2}\|\phi^k\|_2^2, \tag{56}$$

and

$$\begin{aligned}-h^2\big(\hat{\phi}^{k+\frac{1}{2}}\|\phi^{k+1}-\phi^k\big)=&-\frac{1}{2}\|\phi^{k+1}\|_2^2+\frac{1}{4}\|\phi^{k+1}-\phi^k\|_2^2+\frac{1}{2}\|\phi^k\|_2^2-\frac{1}{4}\|\phi^k-\phi^{k-1}\|_2^2\\&+\frac{1}{4}\|\phi^{k+1}-2\phi^k+\phi^{k-1}\|_2^2,\end{aligned} \tag{57}$$

and

$$\begin{aligned}-\big([J\star\hat{\phi}^{k+\frac{1}{2}}]\|\phi^{k+1}-\phi^k\big)=&-\frac{1}{2}\big([J\star\phi^{k+1}]\|\phi^{k+1}\big)+\frac{1}{4}\big([J\star(\phi^{k+1}-\phi^k)]\|\phi^{k+1}-\phi^k\big)\\&+\frac{1}{2}\big([J\star\phi^k]\|\phi^k\big)-\frac{1}{4}\big([J\star(\phi^k-\phi^{k-1})]\|\phi^k-\phi^{k-1}\big)\\&+\frac{1}{4}\big([J\star(\phi^{k+1}-2\phi^k+\phi^{k-1})]\|\phi^{k+1}-2\phi^k+\phi^{k-1}\big).\end{aligned} \tag{58}$$

Now, multiplying Eq. (33) by $w^{k+\frac{1}{2}}$ and using summation-by-parts formulas (see Appendix C), we obtain

$$h^2\big(\phi^{k+1}-\phi^k\|w^{k+\frac{1}{2}}\big)=-s\|\nabla_h w^{k+\frac{1}{2}}\|_M^2. \tag{59}$$

Considering (34), we also have

$$\begin{aligned}h^2\big(\phi^{k+1}-\phi^k\|w^{k+\frac{1}{2}}\big)=&\,h^2\big(\chi(\phi^k,\phi^{k+1})\|\phi^{k+1}-\phi^k\big)+2[J_c\star\mathbf{1}]h^2\big(\phi^{k+\frac{1}{2}}\|\phi^{k+1}-\phi^k\big)\\&-\big(2[J_c\star\mathbf{1}]+\gamma\big)h^2\big(\hat{\phi}^{k+\frac{1}{2}}\|\phi^{k+1}-\phi^k\big)-h^2\big([J\star\hat{\phi}^{k+\frac{1}{2}}]\|\phi^{k+1}-\phi^k\big).\end{aligned} \tag{60}$$

Using identities (55)–(58) in the last equation, we get

$$\begin{aligned}h^2\big(\phi^{k+1}-\phi^k\|w^{k+1}\big)=&\,h^2\big(F_c(\phi^{k+1})\|\mathbf{1}\big)-h^2\big(F_c(\phi^k)\|\mathbf{1}\big)+[J_c\star\mathbf{1}]\|\phi^{k+1}\|_2^2-[J_c\star\mathbf{1}]\|\phi^k\|_2^2\\&-\frac{2[J_c\star\mathbf{1}]+\gamma}{2}\|\phi^{k+1}\|_2^2+\frac{2[J_c\star\mathbf{1}]+\gamma}{4}\|\phi^{k+1}-\phi^k\|_2^2+\frac{2[J_c\star\mathbf{1}]+\gamma}{2}\|\phi^k\|_2^2\\&-\frac{2[J_c\star\mathbf{1}]+\gamma}{4}\|\phi^k-\phi^{k-1}\|_2^2+\frac{2[J_c\star\mathbf{1}]+\gamma}{4}\|\phi^{k+1}-2\phi^k+\phi^{k-1}\|_2^2\\&-\frac{h^2}{2}\big([J\star\phi^{k+1}]\|\phi^{k+1}\big)+\frac{h^2}{4}\big([J\star(\phi^{k+1}-\phi^k)]\|\phi^{k+1}-\phi^k\big)\\&+\frac{h^2}{2}\big([J\star\phi^k]\|\phi^k\big)-\frac{h^2}{4}\big([J\star(\phi^k-\phi^{k-1})]\|\phi^k-\phi^{k-1}\big)\\&+\frac{h^2}{4}\big([J\star(\phi^{k+1}-2\phi^k+\phi^{k-1})]\|\phi^{k+1}-2\phi^k+\phi^{k-1}\big)\\=&\,\mathcal{F}(\phi^k,\phi^{k+1})-\mathcal{F}(\phi^{k-1},\phi^k)+\mathcal{R}(\phi^{k-1},\phi^k,\phi^{k+1}).\end{aligned} \tag{61}$$

It only remains to show that $\mathcal{R}(\phi^{k-1},\phi^k,\phi^{k+1})\geq 0$. On the other hand, by Proposition C.5 and the definition of $\mathcal{R}(\phi^{k-1},\phi^k,\phi^{k+1})$, this fact is straightforward. This proves the result for the nCH scheme. The proof for the nAC scheme is similar and is omitted for the sake of brevity. □

Corollary 3.1. *Suppose that* $\{\phi^{k+1},\mu^{k+\frac{1}{2}}\}_{k=1}^{\ell}\in[\mathcal{C}_{m\times n}]^2$ *are a sequence of periodic solutions pairs of the conservative scheme (33)–(34) or the non-conservative scheme (35)–(36) with the starting values* ϕ^0 *and* ϕ^{-1}*, where* $\phi^{-1}\equiv\phi^0$*. Set* $F_e=\frac{\gamma}{2}\phi^2$ *where* γ *is a nonnegative constant. Then we have*

$$\bar{E}(\phi^k)\leq\bar{E}(\phi^0),\quad\forall 1\leq k\leq\ell. \tag{62}$$

Proof. By virtue of the last theorem, and since $\phi^{-1}\equiv\phi^0$, we have the chain of inequalities

$$\bar{E}(\phi^k)\leq\mathcal{F}(\phi^k)\leq\mathcal{F}(\phi^{k-1})\leq\cdots\leq\mathcal{F}(\phi^0)=\bar{E}(\phi^0). \tag{63}$$ □

Thus, the discrete version of the original energy is bounded from above by the energy of the initial condition.

Table 1
The difference between coarse and fine grid solutions (nCH equation).

Coarse h	Fine h	$\|e_A\|_2$	Rate
1/64	1/128	0.023594977666378	–
1/128	1/256	0.003642747274851	2.695380992993224
1/256	1/512	8.669302357639438e−04	2.071039102165462
1/512	1/1024	2.162606042972027e−04	2.003145023762793
1/1024	1/2048	5.411334233516024e−05	1.998714618858811

Table 2
The difference between coarse and fine grid solutions (nAC equation).

Coarse h	Fine h	$\|e_A\|_2$	Rate
1/64	1/128	1.510704455248701e−04	–
1/128	1/256	3.777326690535997e−05	1.999783979301426
1/256	1/512	9.443660642523572e−06	1.999947459441191
1/512	1/1024	2.360936173440859e−06	1.999987159664891
1/1024	1/2048	5.902355596047761e−07	1.999996293884224

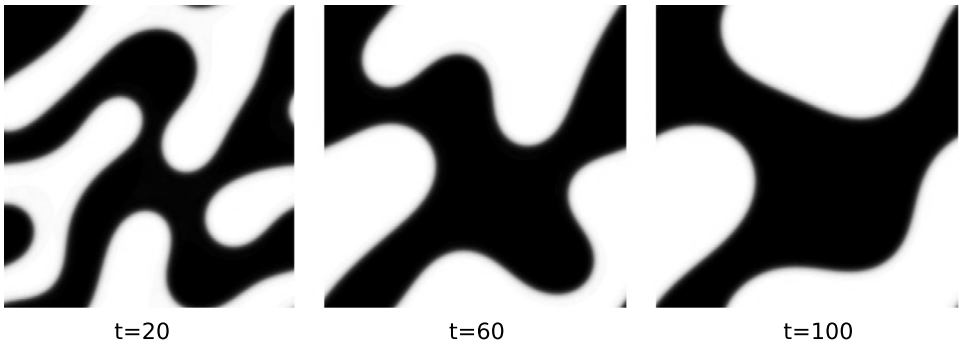

Fig. 1a. Evolution from a random initial condition with $s = 0.01$ (nCH equation).

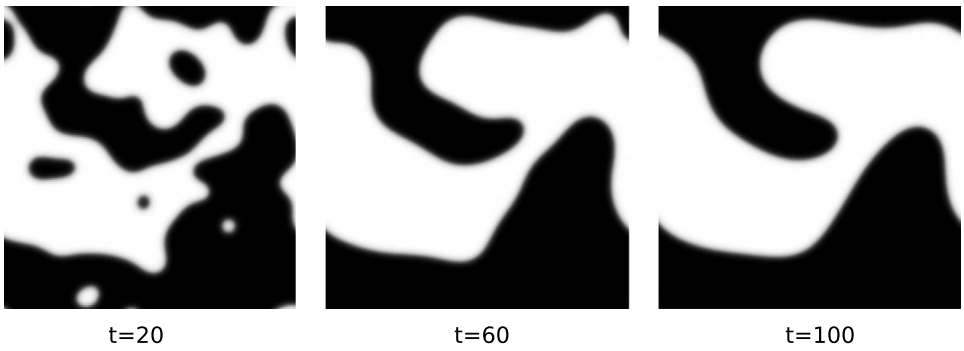

Fig. 1b. Evolution from a random initial condition with $s = 0.01$ (nAC equation).

4. Numerical results

The numerical solution of schemes (33)–(34) and (35)–(36) requires the solution of nonlinear equations at the implicit time level. To solve these nonlinear equations, we use the multigrid solver introduced in [41,54] with small modifications. The reader is also referred to Section 6.2 in [36] for the detailed description of the multigrid method for the first order scheme for the nCH equation which has the similar structure.

4.1. Convergence and stability of second order schemes

In this section we present the results of three numerical experiments verifying the convergence and stability of the proposed schemes. The first experiment verifies the convergence rate in the following setting: **1)** the computation domain is $\Omega = (-0.5, 0.5)^2$; **2)** the initial condition is $\phi(x, 0) = 0.5 \sin(2\pi x_1) \sin(2\pi x_2)$; **3)** the interaction kernel J is given by a positive Gaussian function defined as

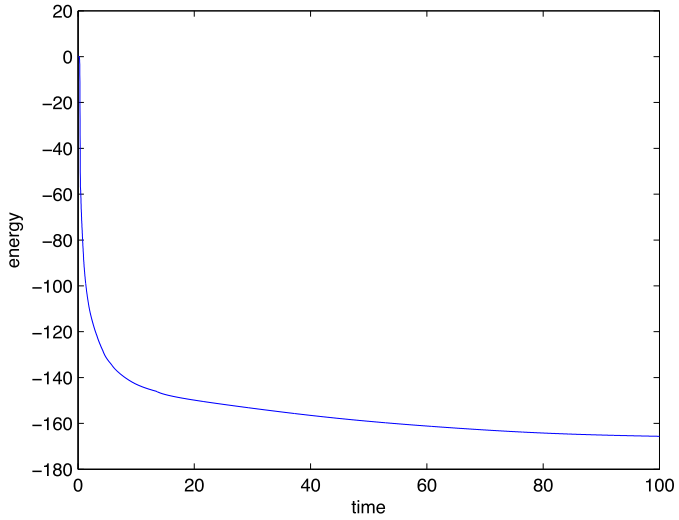

Fig. 2a. Energy of the nCH evolution in Fig. 1a.

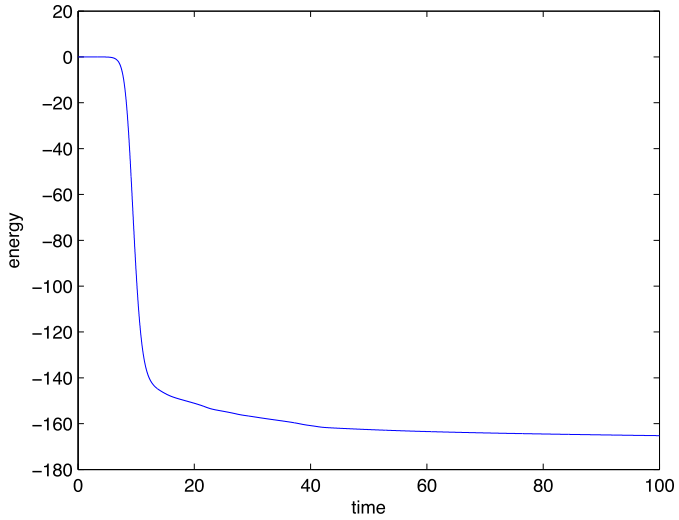

Fig. 2b. Energy of the nAC evolution in Fig. 1b.

$$J = \alpha \exp\left(-\frac{x_1^2 + x_2^2}{\sigma_1^2}\right), \tag{64}$$

where $\sigma_1 = 0.05$ and $\alpha = \frac{1}{\sigma_1^2}$; **4)** $\gamma_e = 1$, $\gamma_c = 0$; **5)** the time step s and the grid size h satisfy the relation $s = 0.1h$; **6)** in all cases, the ending time is 0.015625. Since there is no exact solution to compare with, we use the difference between results on coarse and finer grids to assess accuracy and convergence. Denoting the difference between the results on successively refined grids be e_A, where the fine grid results are averaged to yield values on the coarse grid, the discrete $\|\cdot\|_2$ norm is used to quantify the difference in results [41]. The results are given in Tables 1 and 2 for the nCH (conserved) and nAC (nonconserved) dynamics respectively, and confirm that the schemes are indeed second order accurate. The second experiment is a simulation of spinodal decomposition using the nCH and nAC equations. The setting of the experiment is the following: **1)** $\Omega = (-0.5, 0.5)^2$; **2)** the initial condition is a random perturbation from the initial average $\phi_{ave} = 0$; **3)** J is defined as Eq. (64) with $\sigma_1 = 0.1$ and $\alpha = \frac{1}{\sigma_1^2}$; **4)** $\gamma_e = 1$, $\gamma_c = 0$. Figs. 1a and 1b show the evolving patterns and Figs. 2a and 2b verify the corresponding energy evolution. The third experiment verifies the energy evolution with different sizes of s. Here we use the same setting of the second experiment with the following changes: **1)** the initial condition is $\phi_{t=20}$ obtained in the second experiment and **2)** sizes of s are varied. Figs. 3a and 3b show the evolving patterns with different s. Figs. 4a and 4b show the corresponding energy evolution. Observe that in all cases, their energy decreases with different

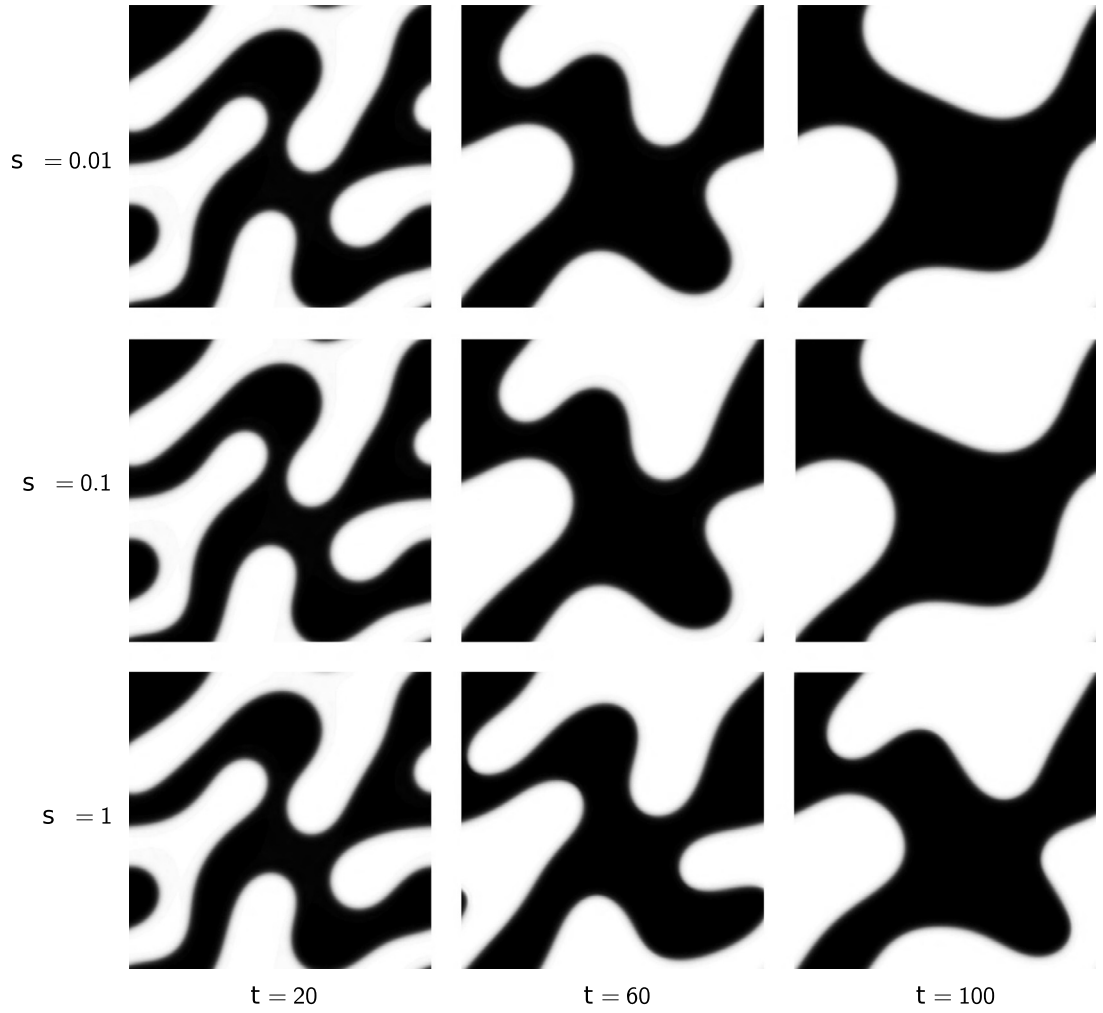

Fig. 3a. Evolving patterns with different s as labeled (nCH equation).

choices of s, and when $s = 0.01$ and $s = 0.1$ the corresponding evolving patterns are very similar. Although when $s = 1$ is used in both nCH and nAC equation, the evolution is less accurate, particularly so for the nCH equation.

4.2. Nucleation and growth

In this section we present two experiments of nucleation and growth described by the nCH equation, where $\Omega = (-10, 10)^2$, $s = 0.01$, the number of nodes on the grid is 512^2, and the total number of time iterations is 10^4. The kernel J is defined as the difference between two Gaussians:

$$J = \alpha \exp\left(-\frac{x_1^2 + x_2^2}{\sigma_1^2}\right) - \beta \exp\left(-\frac{x_1^2 + x_2^2}{\sigma_2^2}\right), \tag{65}$$

where $\sigma_1 = 0.08$, $\sigma_2 = 0.2$, $\alpha = \frac{0.1}{\sigma_1^2}$ and $\beta = \frac{0.09}{\sigma_2^2}$; **4)** $\gamma_e = 0$, $\gamma_c = 0.01$. The contours of J are shown in Fig. 5. In this case $J_c = \alpha \exp(-\frac{x_1^2+x_2^2}{\sigma_1^2})$ and $J_e = \beta \exp(-\frac{x_1^2+x_2^2}{\sigma_2^2})$. The initial condition of the simulation, which is shown in Fig. 6, is a random perturbation of the constant state $\phi_{ave} = 0.2$. Over a short time ($0 \le t \le 10$), the dynamics result in the nucleation of particles (spots) at a fine scale. The corresponding decay of the energy is shown in Fig. 7. In Fig. 8 a second simulation is presented where an initial perturbation of the same state as in Fig. 6 is localized in a small region at the center of the domain. In this case, the nucleation of fine-scale particles starts at the center and radiates outward, while leaving behind defects in the lattice structure. Note that at the outer boundary, curved stripes appear (see $t = 2$ and $t = 4$) that then break up into spots. The reader is referred to [7] for more details concerning the mechanisms underlying the generation of defects in the system.

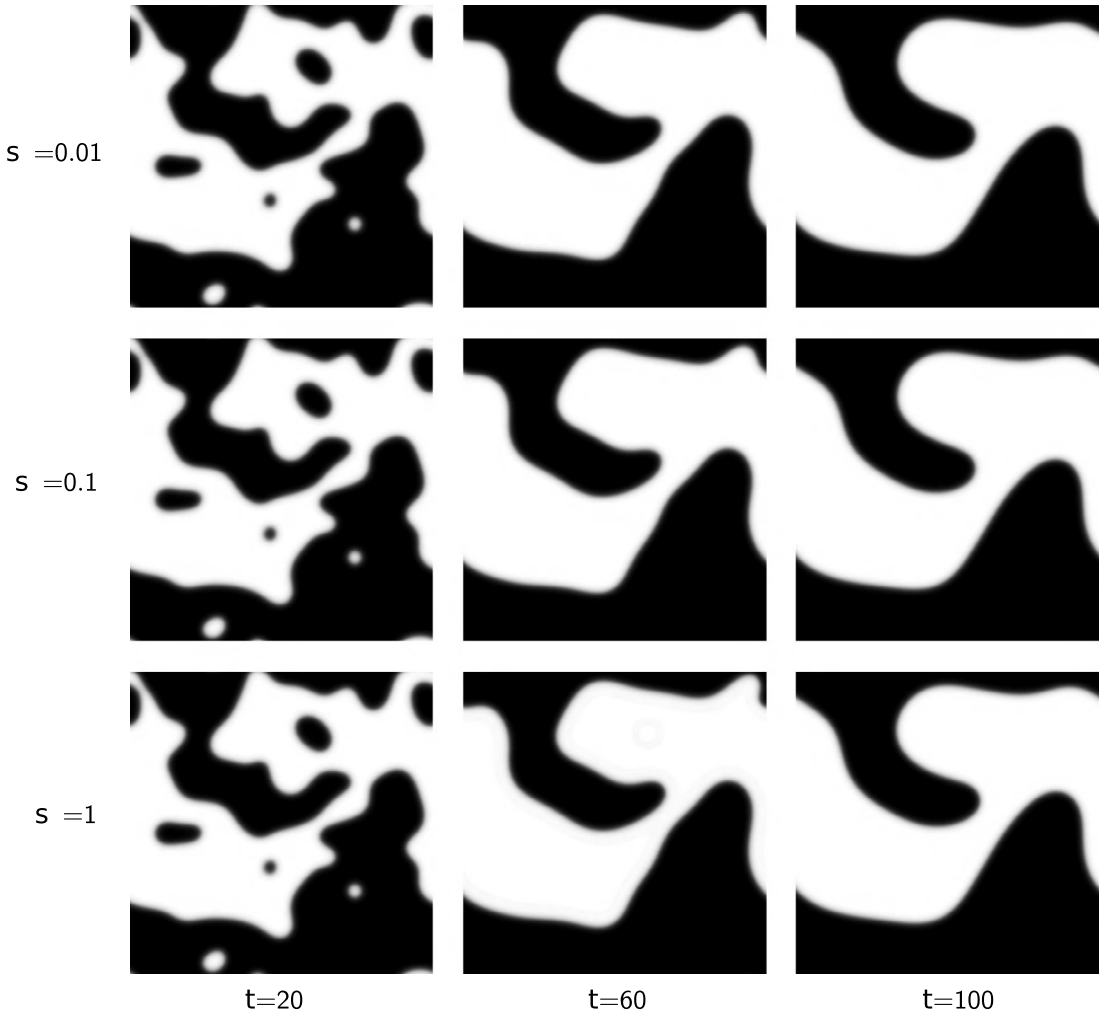

Fig. 3b. Evolving patterns with different s as labeled (nAC equation).

4.3. Efficiency of multigrid solver

To assess the efficiency of the multigrid solver we present the residuals evaluated in the discrete $\|\cdot\|_2$ norm, for each iteration of the V-cycle with $h = 20/2048$, $20/1024$, $20/512$ and $20/256$. We record the residuals at time $t = 0.01$, with $s = 0.01$ for all cases. The initial data is $\phi_0(x, y) = 0.2 + 0.005\sin(200\pi x)\sin(200\pi y)$. The kernel J and the other parameters are as in Section 4.2. The results are given in Fig. 9, which compares the convergence under these settings. We observe that the residual decreases roughly by a constant factor with each V-cycle iteration, independent of the grid size.

4.4. Phase diagram for the nCH equation

In this section we discuss factors that influence nucleation and growth for the nCH equation. In many previous studies it is shown that the average of ϕ is crucial (e.g. [25,35]). It is also clear that the size of the coefficient $\gamma_c - \gamma_e$ is another influential factor. The experiment shown in Fig. 10 is a phase diagram that shows how the equilibrium structures depend on these parameters using the nCH equation. All parameters is the same as Section 4.2 except the following modifications: **1)** the value of parameters for J are $\sigma_1 = 0.08$, $\sigma_2 = 0.2$, $\alpha = \frac{0.1}{\sigma_1^2}$ and $\beta = \frac{0.05}{\sigma_2^2}$; **2)** the averages of ϕ and the parameters $\gamma_c - \gamma_e$ are varied. The initial condition in all cases is a random perturbation of the constant state ϕ_{ave} (which is varied from case to case). The time step s is 0.01 and the total number of time iterations is 5000 for all cases. From Fig. 10 we can see that by increasing the average of ϕ, the pattern changes from labyrinth stripes to dots and eventually to nearly uniform constant. Also we can see from the same figure that when $\gamma_c - \gamma_e$ is increased, the nCH equation is dominated by diffusion and the development of patterns is inhibited.

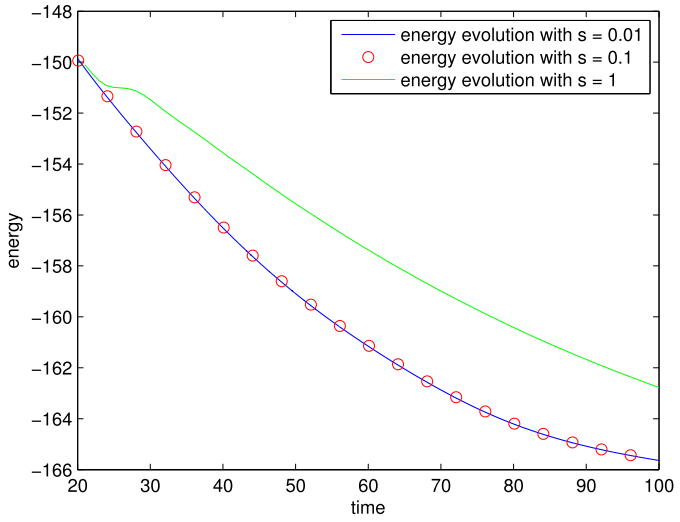

Fig. 4a. Energy of the nCH evolution in Fig. 3a. (For interpretation of the references to color in this figure, the reader is referred to the web version of this article.)

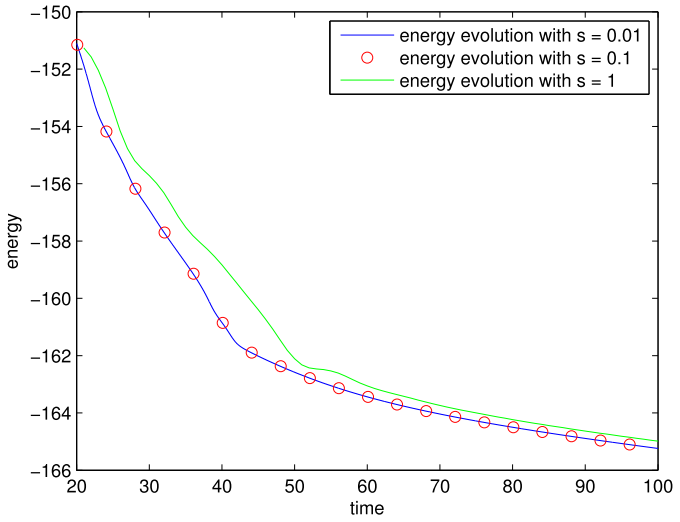

Fig. 4b. Energy of the nAC evolution in Fig. 3b. (For interpretation of the references to color in this figure, the reader is referred to the web version of this article.)

4.5. Nucleation and growth with anisotropic interaction kernels

In this section we discuss the influence of the structure of J on nucleation and growth in the nCH equation. We consider four interaction kernels J_1, J_2, J_3 and J_4, which are defined as:

$$J_1 = \alpha \exp\left(-\frac{x_1^2+x_2^2}{\sigma_1^2}\right) - \beta \exp\left(-\frac{x_1^2+x_2^2}{\sigma_2^2}\right), \tag{66}$$

$$\begin{aligned} J_2 = {} & 0.5\alpha\left[\exp\left(-\frac{x_1^2}{(0.5\sigma_1)^2}-\frac{x_2^2}{\sigma_1^2}\right)+\exp\left(-\frac{x_1^2}{\sigma_1^2}-\frac{x_2^2}{(0.5\sigma_1)^2}\right)\right] \\ & - 0.5\beta\left[\exp\left(-\frac{x_1^2}{(0.5\sigma_2)^2}-\frac{x_2^2}{\sigma_2^2}\right)+\exp\left(-\frac{x_1^2}{\sigma_2^2}-\frac{x_2^2}{(0.5\sigma_2)^2}\right)\right], \end{aligned} \tag{67}$$

$$\begin{aligned} J_3 = {} & 0.5\alpha\left[\exp\left(-\frac{0.5(x_1-x_2)^2}{(0.5\sigma_1)^2}-\frac{0.5(x_1+x_2)^2}{\sigma_1^2}\right)+\exp\left(-\frac{0.5(x_1-x_2)^2}{\sigma_1^2}-\frac{0.5(x_1+x_2)^2}{(0.5\sigma_1)^2}\right)\right] \\ & - 0.5\beta\left[\exp\left(-\frac{0.5(x_1-x_2)^2}{(0.5\sigma_2)^2}-\frac{0.5(x_1+x_2)^2}{\sigma_2^2}\right)+\exp\left(-\frac{0.5(x_1-x_2)^2}{\sigma_2^2}-\frac{0.5(x_1+x_2)^2}{(0.5\sigma_2)^2}\right)\right], \end{aligned} \tag{68}$$

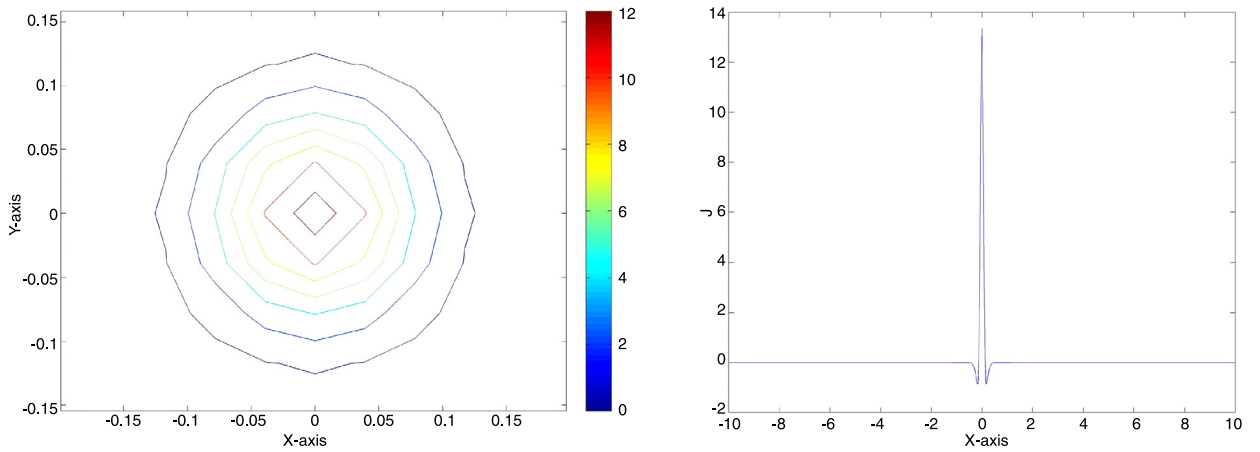

Fig. 5. The interaction kernel J given in Eq. (65) and used in the simulation shown in Fig. 6. The left figure shows the contour. The right figure is a cut view at $y = 0$. (For interpretation of the references to color in this figure, the reader is referred to the web version of this article.)

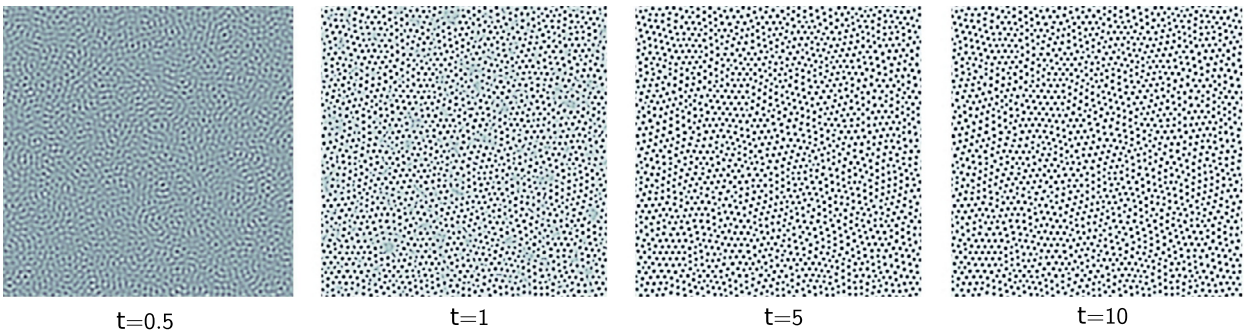

Fig. 6. Dynamics for the nCH equation with a random initial condition and interaction kernel J shown in Fig. 5.

$$
\begin{aligned}
J_4 = {} & \frac{\alpha}{3}\exp\left(-\frac{x_1^2}{\sigma_1^2} - \frac{x_2^2}{(0.5\sigma_1)^2}\right) + \frac{\alpha}{3}\exp\left(-\frac{(\frac{1}{2}x_1 - \frac{\sqrt{3}}{2}x_2)^2}{\sigma_1^2} - \frac{(\frac{\sqrt{3}}{2}x_1 + \frac{1}{2}x_2)^2}{(0.5\sigma_1)^2}\right) \\
& + \frac{\alpha}{3}\exp\left(-\frac{(\frac{1}{2}x_1 - \frac{\sqrt{3}}{2}x_2)^2}{\sigma_1^2} - \frac{(\frac{\sqrt{3}}{2}x_1 - \frac{1}{2}x_2)^2}{(0.5\sigma_1)^2}\right) \\
& - \frac{\beta}{3}\exp\left(-\frac{x_1^2}{\sigma_2^2} - \frac{x_2^2}{(0.5\sigma_2)^2}\right) - \frac{\beta}{3}\exp\left(-\frac{(\frac{1}{2}x_1 - \frac{\sqrt{3}}{2}x_2)^2}{\sigma_2^2} - \frac{(\frac{\sqrt{3}}{2}x_1 + \frac{1}{2}x_2)^2}{(0.5\sigma_2)^2}\right) \\
& - \frac{\beta}{3}\exp\left(-\frac{(\frac{1}{2}x_1 - \frac{\sqrt{3}}{2}x_2)^2}{\sigma_2^2} - \frac{(\frac{\sqrt{3}}{2}x_1 - \frac{1}{2}x_2)^2}{(0.5\sigma_2)^2}\right),
\end{aligned} \tag{69}
$$

where $\sigma_1 = 0.16$, $\sigma_2 = 0.4$, $\alpha = \frac{0.1}{\sigma_1^2}$ and $\beta = \frac{0.08}{\sigma_2^2}$. Figs. 11a, 11b, 11c and 11d show the contours of the Js. In Fig. 12 the evolution of ϕ from a randomly perturbed average $\phi_{ave} = 0.19$, which is localized to a small region in the center of the domain, are shown for different kernels. The computational domain is $\Omega = (-10, 10)^2$ and the value of $\gamma_c - \gamma_e$ is 0. As seen in the figure the microstructure of growth very clearly depends on J.

Remark 4.1. The interaction kernel J_4 has six-fold anisotropic shape, and the nucleation and growth simulation in this setting is very similar to the simulation of the anisotropic PFC equation presented in [21].

In Figs. 13a and 13b, we close with a simulation that resembles microphase separation [4,42–44,53]. In Fig. 13a the interaction kernel $J = J_1$, as in the previous section, with $\sigma_1 = 0.08$, $\sigma_2 = 0.2$, $\alpha = \frac{0.5}{\sigma_1^2}$ and $\beta = \frac{0.25}{\sigma_2^2}$; $\gamma_e = 0$, $\gamma_c = 0$. The computational domain is $\Omega = (-20, 20)^2$ and the initial condition is a random perturbation of the constant state $\phi = \phi_{ave} = 0.3$ localized in a small region of the center of the domain. Observe that blocks of patterned structures emerge

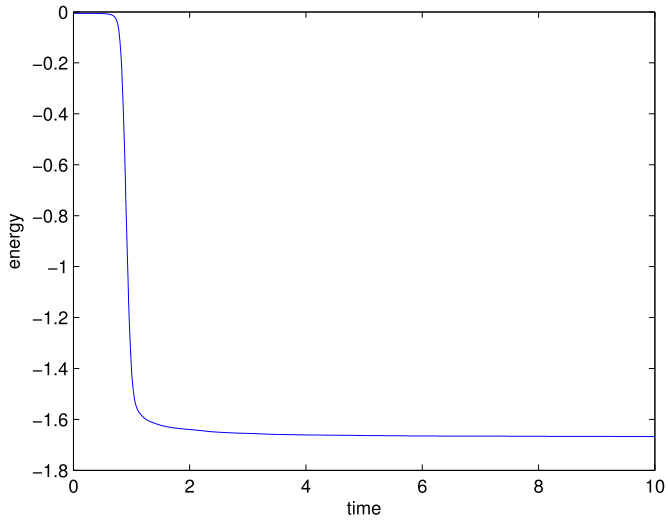

Fig. 7. The corresponding energy for the simulation shown in Fig. 6.

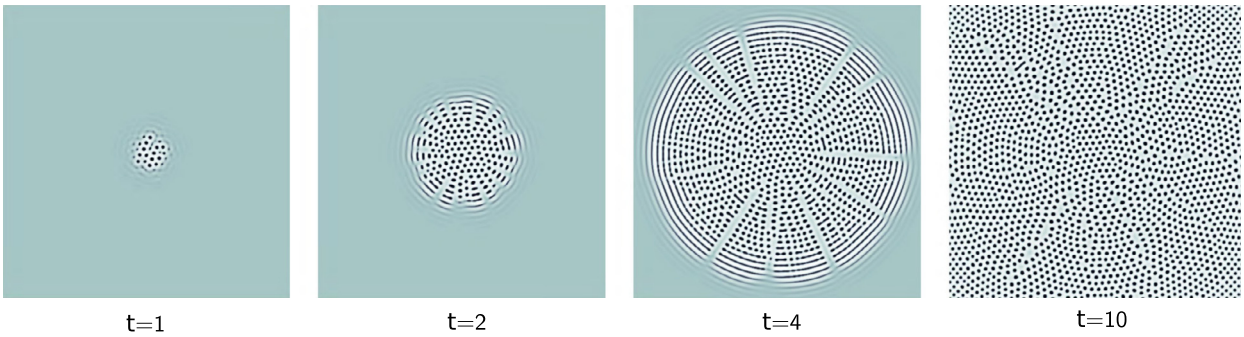

Fig. 8. Nucleation and growth from a random initial perturbation in a small region at the center of the domain. The interaction kernel J is that shown in Fig. 5.

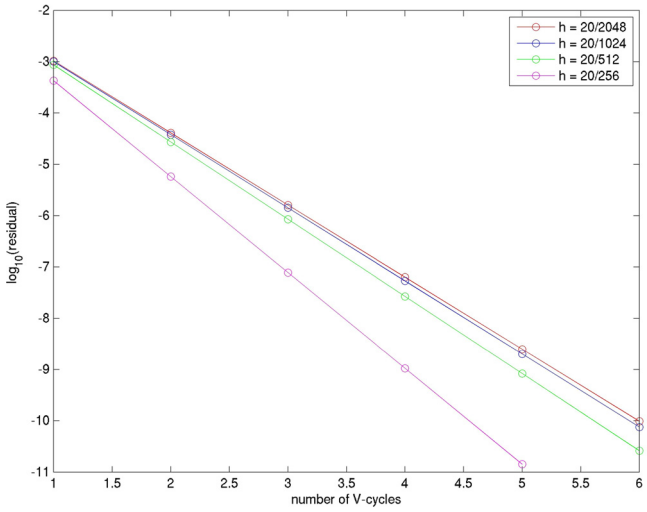

Fig. 9. Logarithm of residual against number of V-cycle in multigrid solver. (For interpretation of the references to color in this figure, the reader is referred to the web version of this article.)

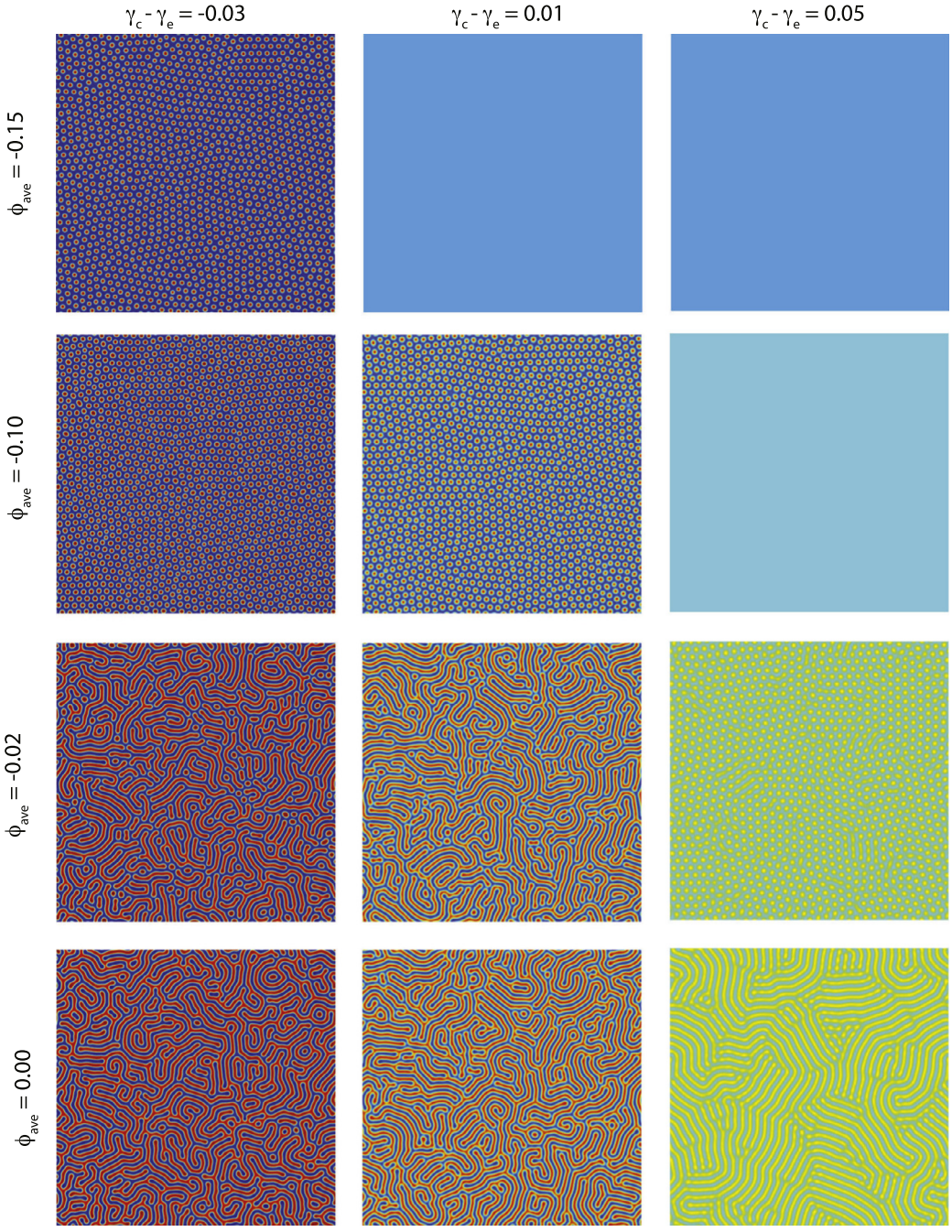

Fig. 10. The phase diagram for the nCH equation with different ϕ_{ave} and $\gamma_c - \gamma_e$. The simulations are shown at the same time $t = 50$.

distributed radically from the center of the domain. Over time, some of these structures merge to form patterned rings of stripes. Such structures have been observedexperimentally [53]. In Fig. 13b analogous simulations are performed using the interaction kernel $J = J_4$. In this case $\sigma_1 = 0.15$, $\sigma_2 = 0.375$, $\alpha = \frac{0.5}{\sigma_1^2}$ and $\beta = \frac{0.25}{\sigma_2^2}$; $\gamma_e = 0$, $\gamma_c = 0$. The computational domain is $\Omega = (-40, 40)^2$ and the initial condition is a random perturbation of the constant state $\phi = \phi_{ave} = 0.288$ localized in a small region of the center of the domain. The corresponding evolution is qualitatively similar to that observed in Fig. 13a, although the details of the pattern (spots) and the stripes (which have not fully formed) are different and influenced by the interaction kernel.

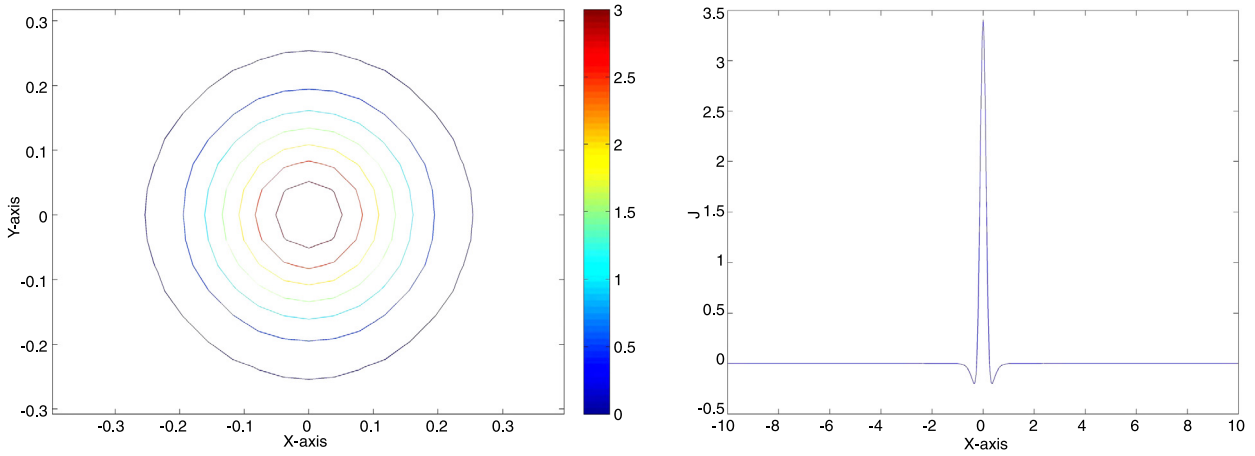

Fig. 11a. The isotropic interaction kernel J_1. The left figure shows the contours. The right figure is a cut view at $y = 0$. (For interpretation of the colors in this figure, the reader is referred to the web version of this article.)

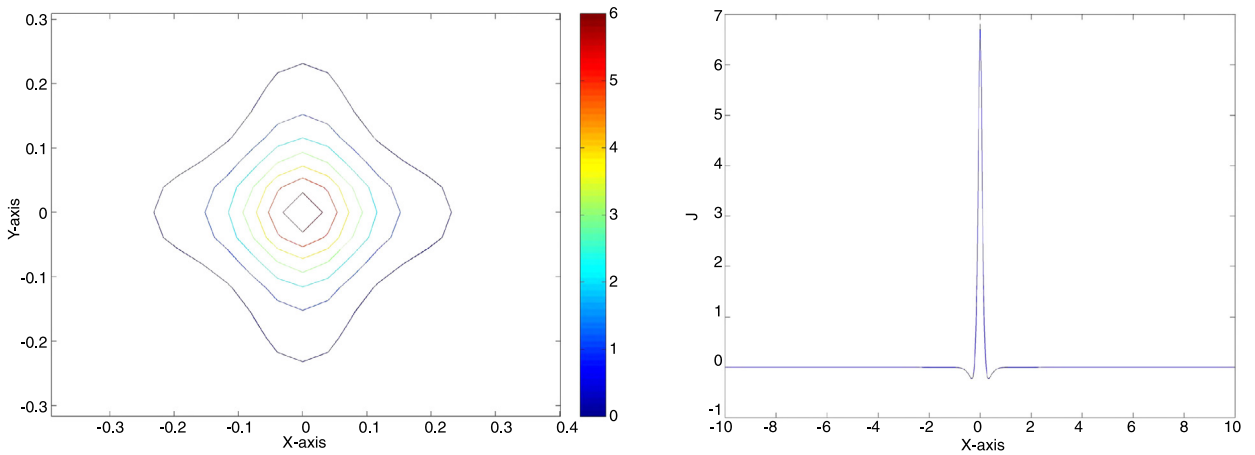

Fig. 11b. The anisotropic interaction kernel J_2. The left figure shows the contours. The right figure is a cut view at $y = 0$. (For interpretation of the colors in this figure, the reader is referred to the web version of this article.)

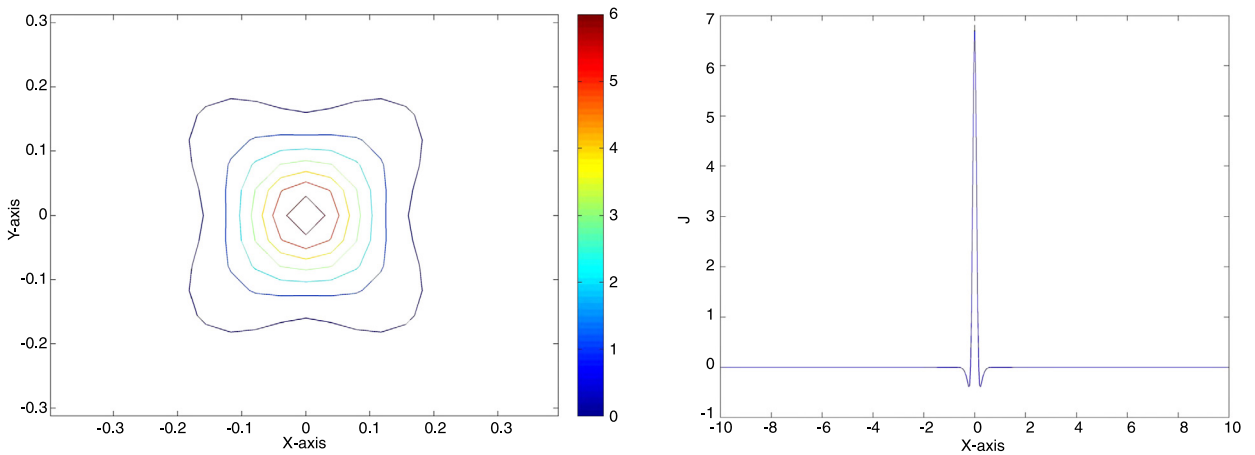

Fig. 11c. The anisotropic interaction kernel J_3. The left figure shows the contours. The right figure is a cut view at $y = 0$. (For interpretation of the colors in this figure, the reader is referred to the web version of this article.)

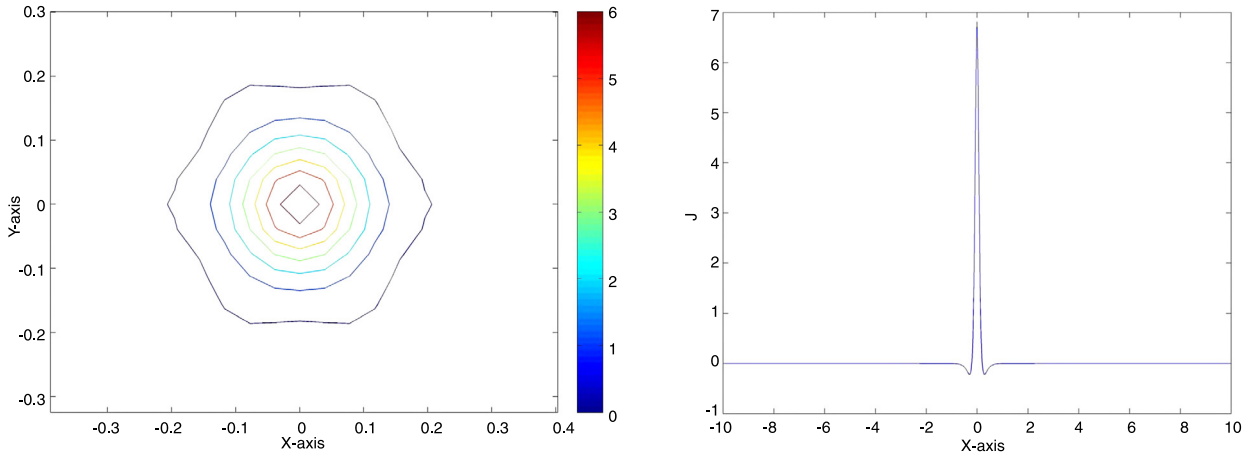

Fig. 11d. The anisotropic interaction kernel J_4. The left figure shows the contours. The right figure is a cut view at $y = 0$. (For interpretation of the colors in this figure, the reader is referred to the web version of this article.)

5. Conclusion and future work

In this paper we have presented second-order accurate unconditionally energy stable finite difference schemes for integro-partial–differential nonlocal Cahn–Hilliard and Allen–Cahn equations. Although the equations at the implicit time level are nonlinear, our schemes are uniquely solvable for any time step using a finite difference/volume discretization in space. The excellent performance of our schemes is demonstrated by simulating a variety of different configurations.

Our immediate plan is to apply this scheme to equations that arise in dynamic density functional theory to achieve more efficient simulation algorithms than currently exist. Another plan is to develop an adaptive time-stepping scheme where the value of s is adjusted at each time iteration to take the advantage of unconditional energy stability, like scheme described in [58]. In addition we also plan to develop a parallel version of this solver. In practice the size of the problem is much larger than the test cases we presented here, and large scale 3D simulations are beyond the capability of a single computer. Finally, we also plan to adapt the ideas presented here to finite element schemes.

Acknowledgements

J.L. acknowledges partial support from NSF-CHE 1035218, NSF-DMR 1105409 and NSF-DMS 1217273. C.W. acknowledges partial support from NSF-DMS 1115420, NSF-DMS 1418689, NSF-DCNS 0959382, AFOSR-10418149 and NSFC 11271281. S.M.W. acknowledges partial support from NSF-DMS 1115390.

Appendix A. Relationship between the circular and classical convolutions

The classical convolution operation is widely used in many applications, including DDFT. In practice this convolution is often approximated by the circular convolution in a bounded, rectangular domain. Here, we very briefly discuss the relationship between the classical and circular convolutions in one space dimension. This can be extended naturally to higher dimensions. Here we give only a formal description, but a more rigorous approach can be found in [40] and elsewhere.

Suppose that $\phi : \mathbb{R} \to \mathbb{R}$ is a sufficiently regular L-periodic function, $L > 0$, and $J : \mathbb{R} \to \mathbb{R}$ is a sufficiently regular, even convolution kernel, $J(-x) = J(x)$ with sufficiently rapid decay at infinity. Note that J is not assumed to be periodic. The convolution on $\mathbb{R}$ is

$$(J * \phi)(x) = \int_{\mathbb{R}} J(x-y)\phi(y)\,dy = \int_{\mathbb{R}} J(y)\phi(x-y)\,dy. \tag{70}$$

Now, using the periodicity of ϕ,

$$\begin{aligned}(J * \phi)(x) &= \sum_{k=-\infty}^{\infty} \int_{kL}^{(k+1)L} J(x-y)\phi(y)\,dy = \sum_{k=-\infty}^{\infty} \int_{0}^{L} J(x-y-kL)\phi(y)\,dy \\ &= \int_{0}^{L} \sum_{k=-\infty}^{\infty} J(x-y-kL)\phi(y)\,dy. \end{aligned} \tag{71}$$

We define the periodic sum of J as

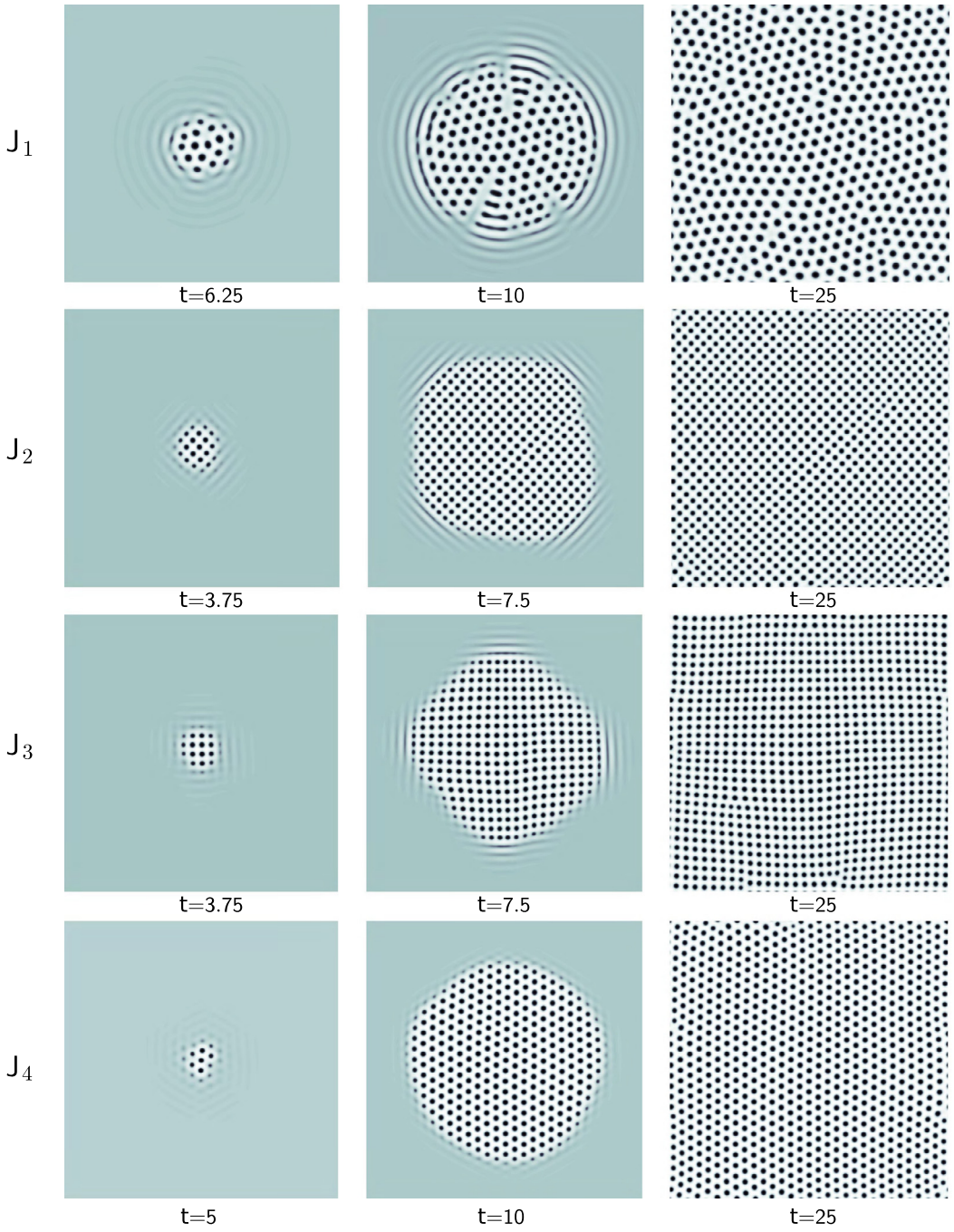

Fig. 12. Nucleation and growth resulting from a small random perturbation at the center of the domain using different interaction kernels as labeled.

$$J_p(x) := \sum_{k=-\infty}^{\infty} J(x - kL). \tag{72}$$

Observe that, J_p is L-periodic and even. Moreover if the original convolution kernel J has compact support in $(-L/2, L/2)$, then J_p is merely the periodic extension of J from $[-L/2, L/2]$ to the whole real line. With our definition, we have

$$(J * \phi)(x) = \int_0^L J_p(x - y)\phi(y)\, dy = \int_0^L J_p(y)\phi(x - y)\, dy. \tag{73}$$

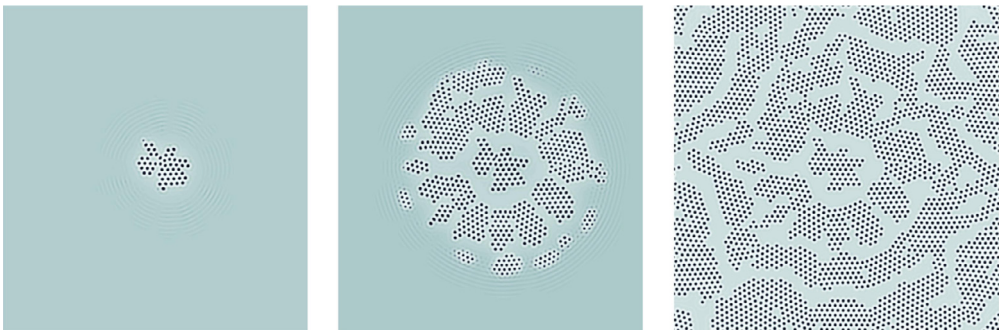

Fig. 13a. Microphase separation using the isotropic interaction kernel J_1.

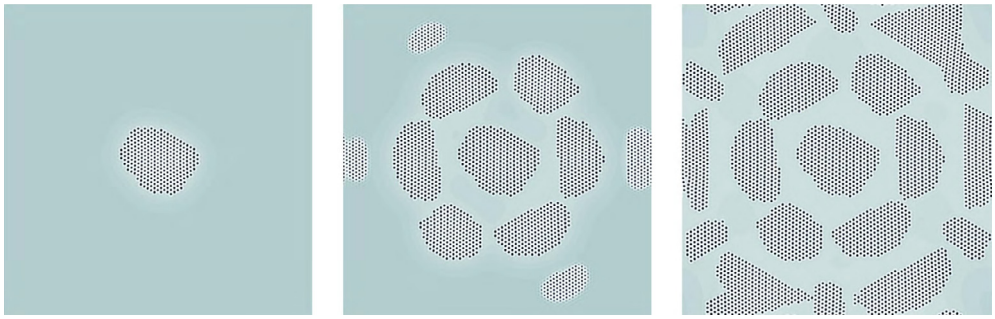

Fig. 13b. Microphase separation using the six-fold interaction kernel J_4.

In materials science applications, it is usually a quite reasonable assumption to model J as having compact support and ϕ as being periodic, especially when dealing with "bulk" material properties, such as bulk phase transition. However, when boundary effects become important, one should switch to a more realistic model that avoids the periodicity assumption, such as those considered by Bates et al. [12–16]. For the computations herein, for simplicity, we usually take J to be a Gaussian, which can be a good approximation of a compactly supported kernel when the peak is sufficiently narrow. See, for example, Figs. 11a–11d.

Appendix B. Regularization of regular solution model free energy

The ideal part of regular solution model free energy is defined as Eq. (15), thus ϕ needs to satisfies $0 < \phi < 1$ for both the well posedness of the problem and the convexity of the energy. However, the second order scheme (33)–(34) for the nCH equation and the second order scheme (35)–(36) for the nAC equation do not necessarily preserve positivity. Our primary goal here is to present an approximation for Eq. (15) that fits the framework of this paper.

We consider the following approximation of Eq. (15):

$$F_\nu(\phi) := \theta\Big[\sqrt{\phi^2+\nu^2}\log\Big(\sqrt{\phi^2+\nu^2}\Big) + \sqrt{(1-\phi)^2+\nu^2}\log\Big(\sqrt{(1-\phi)^2+\nu^2}\Big)\Big] - 2\theta_c\phi(1-\phi), \tag{74}$$

where ν is a scalar, we set

$$F_\nu = F_c - F_e \tag{75}$$

where

$$F_c = F_\nu + \Upsilon(\nu)\phi^2 \tag{76}$$

and

$$F_e = \Upsilon(\nu)\phi^2, \tag{77}$$

provided θ and θ_c are positive. $\Upsilon(\nu)$ is a positive constant that is inversely proportional to ν.

It can be proved that for $0 < \phi < 1$,

$$\lim_{\nu\to 0} F_\nu(\phi) = \theta\big[\phi\log(\phi) + (1-\phi)\log(1-\phi)\big] - 2\theta_c\phi(1-\phi) \tag{78}$$

point-wise. It can also be proved that $F_\nu + \Upsilon(\nu)\phi^2$ and $\Upsilon(\nu)\phi^2$ are convex. Therefore Eq. (74) can be used as an approximation of Eq. (15) while satisfying Eq. (13) for any ϕ. Thus corresponding unconditionally energy stable schemes can be derived. However, it needs to be pointed out that in the application of schemes (23)–(24) and (26)–(27), $F_\nu(\phi)$ will introduce extra numerical error in the term

$$\Upsilon(\nu)\phi^{n+\frac{1}{2}} - \Upsilon(\nu)\hat{\phi}^{n+\frac{1}{2}} \tag{79}$$

since $F_c(\phi)$ is treated implicitly and $F_e(\phi)$ is treated explicitly. The size of the error is proportional to the size of $\Upsilon(\nu)$. Thus if we decrease the size of ν to achieve a better approximation of Eq. (15), the error in the numerical simulations may increase.

Appendix C. Discretization of two-dimensional space

Our primary goal in this appendix is to define some finite-difference operators and provide some summation-by-parts formulas in two-dimension that are used to derive and analyze the numerical schemes. The theory and algorithms extend straightforwardly to three-dimension.

For simplicity, let us assume that $\Omega = (0, L_1) \times (0, L_2)$. Here we use the notation and results for cell-centered functions from [56,54]. The reader is directed to those references for more complete details. We begin with definitions of grid functions and difference operators needed for our discretization of two-dimensional space. Let $\Omega = (0, L_1) \times (0, L_2)$, with $L_1 = m \cdot h$ and $L_2 = n \cdot h$, where m and n are positive integers and $h > 0$ is the spatial step size. Define $x_i := (i - \frac{1}{2}) \cdot h$, where i takes on integer and half-integer values. For any positive integer ℓ, define $E_\ell = \{x_i \mid i = \frac{1}{2}, \ldots, \ell + \frac{1}{2}\}$, $C_\ell = \{x_i \mid i = 1, \ldots, \ell\}$, $C_{\bar{\ell}} = \{x_i \mid i = 0, \ldots, \ell + 1\}$. The positions y_j can be defined in the same fashion. Define the function spaces

$$\mathcal{C}_{m\times n} = \{\phi : C_m \times C_n \to \mathbb{R}\}, \qquad \mathcal{C}_{\bar{m}\times\bar{n}} = \{\phi : C_{\bar{m}} \times C_{\bar{n}} \to \mathbb{R}\}, \tag{80}$$

$$\mathcal{E}^{ew}_{m\times n} = \{u : E_m \times C_n \to \mathbb{R}\}, \qquad \mathcal{E}^{ns}_{m\times n} = \{v : C_m \times E_n \to \mathbb{R}\}, \tag{81}$$

$$\mathcal{E}^{ew}_{m\times\bar{n}} = \{u : E_m \times C_{\bar{n}} \to \mathbb{R}\}, \qquad \mathcal{E}^{ns}_{\bar{m}\times n} = \{v : C_{\bar{m}} \times E_n \to \mathbb{R}\}, \tag{82}$$

$$\mathcal{V}_{m\times n} = \{f : E_m \times E_n \to \mathbb{R}\}. \tag{83}$$

We use the notation $\phi_{i,j} := \phi(x_i, y_j)$ for *cell-centered* functions (those in the spaces $\mathcal{C}_{m\times n}$ or $\mathcal{C}_{\bar{m}\times\bar{n}}$). In component form *east–west edge-centered* functions, those in the spaces $\mathcal{E}^{ew}_{m\times n}$ or $\mathcal{E}^{ew}_{m\times\bar{n}}$, are identified via $u_{i+\frac{1}{2},j} := u(x_{i+\frac{1}{2}}, y_j)$. In component form *north–south edge-centered* functions, those in the spaces $\mathcal{E}^{ns}_{m\times n}$, or $\mathcal{E}^{\mathrm{ns}}_{\bar{m}\times n}$, are identified via $u_{i+\frac{1}{2},j} := u(x_{i+\frac{1}{2}}, y_j)$. The functions of $\mathcal{V}_{m\times n}$ are called *vertex-centered* functions. In component form vertex-centered functions are identified via $f_{i+\frac{1}{2},j+\frac{1}{2}} := f(x_{i+\frac{1}{2}}, y_{j+\frac{1}{2}})$.

We will need the weighted 2D discrete inner-products $(\cdot\|\cdot)$, $[\cdot\|\cdot]_{ew}$, $[\cdot\|\cdot]_{ns}$ that are defined in [56,54]:

$$(\phi\|\psi) = \sum_{i=1}^{m}\sum_{j=1}^{n}\phi_{i,j}\psi_{i,j}, \quad \phi, \psi \in \mathcal{C}_{m\times n} \cup \mathcal{C}_{\bar{m}\times\bar{n}}, \tag{84}$$

$$[f\|g]_{ew} = \frac{1}{2}\sum_{i=1}^{m}\sum_{j=1}^{n}(f_{i+\frac{1}{2},j}g_{i+\frac{1}{2},j} + f_{i-\frac{1}{2},j}g_{i-\frac{1}{2},j}), \quad f, g \in \mathcal{E}^{ew}_{m\times n}, \tag{85}$$

$$[f\|g]_{ns} = \frac{1}{2}\sum_{i=1}^{m}\sum_{j=1}^{n}(f_{i,j+\frac{1}{2}}g_{i,j+\frac{1}{2}} + f_{i,j-\frac{1}{2}}g_{i,j-\frac{1}{2}}), \quad f, g \in \mathcal{E}^{ns}_{m\times n}. \tag{86}$$

In addition to these, we will use the 2D discrete inner product

$$\begin{aligned}\langle f\|g\rangle = \frac{1}{4}\sum_{i=1}^{m}\sum_{j=1}^{n}(&f_{i+\frac{1}{2},j+\frac{1}{2}}g_{i+\frac{1}{2},j+\frac{1}{2}} + f_{i+\frac{1}{2},j-\frac{1}{2}}g_{i+\frac{1}{2},j-\frac{1}{2}}\\ &+ f_{i-\frac{1}{2},j+\frac{1}{2}}g_{i-\frac{1}{2},j+\frac{1}{2}} + f_{i-\frac{1}{2},j-\frac{1}{2}}g_{i-\frac{1}{2},j-\frac{1}{2}}), \quad f, g \in \mathcal{V}^{ns}_{m\times n}.\end{aligned} \tag{87}$$

Following [56,54], the edge-to-center differences, $d_x : \mathcal{E}^{ew}_{m\times n} \to \mathcal{C}_{m\times n}$ and $d_y : \mathcal{E}^{\mathrm{ns}}_{m\times n} \to \mathcal{C}_{m\times n}$; the center-to-edge averages and differences, $A_x, D_x : \mathcal{C}_{\bar{m}\times n} \to \mathcal{E}^{ew}_{m\times n}$ and $A_y, D_y : \mathcal{C}_{m\times\bar{n}} \to \mathcal{E}^{ew}_{m\times n}$; and the 2D discrete Laplacian, $\Delta_h : \mathcal{C}_{\bar{m}\times\bar{n}} \to \mathcal{C}_{m\times n}$ are defined component-wise via

$$d_x f_{i,j} = \frac{1}{h}(f_{i+\frac{1}{2},j} - f_{i-\frac{1}{2},j}), \qquad d_y f_{i,j} = \frac{1}{h}(f_{i,j+\frac{1}{2}} - f_{i,j-\frac{1}{2}}), \quad \begin{matrix} i=1,\ldots,m \\ j=1,\ldots,n \end{matrix}, \tag{88}$$

$$A_x\phi_{i+\frac{1}{2},j} = \frac{1}{2}(\phi_{i,j} + \phi_{i+1,j}), \qquad D_x\phi_{i+\frac{1}{2},j} = \frac{1}{h}(\phi_{i+1,j} - \phi_{i,j}), \quad \begin{matrix} i=0,\ldots,m \\ j=1,\ldots,n \end{matrix}, \tag{89}$$

$$A_y\phi_{i,j+\frac{1}{2}} = \frac{1}{2}(\phi_{i,j} + \phi_{i,j+1}), \qquad D_y\phi_{i,j+\frac{1}{2}} = \frac{1}{h}(\phi_{i,j+1} - \phi_{i,j}), \quad \begin{matrix} i=1,\dots,m \\ j=0,\dots,n \end{matrix}, \tag{90}$$

$$\Delta_h\psi_{i,j} = d_x(D_x\psi)_{i,j} + d_y(D_y\psi)_{i,j}, \quad \begin{matrix} i=1,\dots,m \\ j=1,\dots,n \end{matrix}. \tag{91}$$

We shall say the cell-centered function $\phi \in \mathcal{C}_{m\times n}$ is periodic if and only if, for all $p, q \in \mathbb{Z}$,

$$\phi_{i+p\cdot m, j+q\cdot n} = \phi_{i,j}, \quad i = 1,\dots,m,\ j = 1,\dots,n. \tag{92}$$

Here we have abused notation a bit, since ϕ is not explicitly defined on an infinite grid. Of course, ϕ can be extended as a periodic function in a natural way, which is the context in which we view the last definition. Similar definitions are available for periodic edge and vertex centered grid functions.

We will use the grid function norms defined in [56,54]. The reader is referred to those references for the precise definitions of $\|\cdot\|_2$, $\|\cdot\|_\infty$, $\|\cdot\|_p$ $(1 \le p < \infty)$, $\|\cdot\|_{0,2}$, $\|\cdot\|_{1,2}$, and $\|\phi\|_{2,2}$.

Using the definitions given in this appendix and in [56,54], we obtain the following summation-by-parts formulas whose proofs are simple:

Proposition C.1 *(Summation-by-parts). If $\phi \in \mathcal{C}_{\bar{m}\times\bar{n}}$ is periodic and $f \in \mathcal{E}^{ew}_{m\times n}$ is periodic then*

$$h^2\,[D_x\phi\|f]_{ew} = -h^2\,(\phi\|d_x f), \tag{93}$$

and if $\phi \in \mathcal{C}_{\bar{m}\times\bar{n}}$ is periodic and $f \in \mathcal{E}^{ns}_{m\times n}$ is periodic then

$$h^2\,[D_y\phi\|f]_{ns} = -h^2\,(\phi\|d_y f). \tag{94}$$

If $f \in \mathcal{V}_{m\times n}$ is periodic and $g \in \mathcal{E}^{ns}_{\bar{m}\times n}$ is periodic then

$$h^2\cdot[d_x f\|g]_{ns} = -h^2\cdot\langle f\|D_x g\rangle, \tag{95}$$

and if $f \in \mathcal{V}_{m\times n}$ is periodic and $g \in \mathcal{E}^{ew}_{m\times\bar{n}}$ is periodic then

$$h^2\cdot[d_y f\|g]_{ew} = -h^2\cdot\langle f\|D_y g\rangle. \tag{96}$$

Proposition C.2 *(Discrete Green's first identity). Let $\phi,\ \psi \in \mathcal{C}_{\bar{m}\times\bar{n}}$ be periodic grid functions. Then*

$$h^2\,[D_x\phi\|D_x\psi]_{ew} + h^2\,[D_y\phi\|D_y\psi]_{ns} = -h^2\,(\phi\|\Delta_h\psi). \tag{97}$$

Proposition C.3 *(Discrete Green's second identity). Let $\phi,\ \psi \in \mathcal{C}_{\bar{m}\times\bar{n}}$ be periodic grid functions. Then*

$$h^2\,(\phi\|\Delta_h\psi) = h^2\,(\Delta_h\phi\|\psi). \tag{98}$$

We need to define a discrete periodic convolution operator. Suppose $\phi \in \mathcal{C}_{m\times n}$ is periodic and $\varphi \in \mathcal{V}_{m\times n}$ is periodic. Then the discrete convolution operator $[\varphi\star\phi] : \mathcal{V}_{m\times n}\times\mathcal{C}_{m\times n} \to \mathcal{C}_{m\times n}$ is defined component-wise as

$$[\varphi\star\phi]_{i,j} = h^2\sum_{k=1}^{m}\sum_{l=1}^{n}\varphi_{k+\frac{1}{2},l+\frac{1}{2}}\phi_{i-k,j-l}. \tag{99}$$

Notice very carefully that order is important in the definition of the discrete convolution $[\cdot\star\cdot]$

Proposition C.4. *If $\phi \in \mathcal{C}_{m\times n}$ is periodic and $\varphi \in \mathcal{V}_{m\times n}$ is periodic, then*

$$[\varphi\star\phi]_{i,j} = h^2\sum_{k=1}^{m}\sum_{l=1}^{n}\varphi_{i-k+\frac{1}{2},j-l+\frac{1}{2}}\phi_{k,l}. \tag{100}$$

Proposition C.5. *If $\phi,\ \psi \in \mathcal{C}_{m\times n}$ are periodic and $\varphi \in \mathcal{V}_{m\times n}$ is even, non-negative, and periodic, then, for any $\alpha > 0$,*

$$\left|\left(\phi\middle\|[\varphi\star\psi]\right)\right| \le \frac{\alpha}{2}[\varphi\star\mathbf{1}](\phi\|\phi) + \frac{1}{2\alpha}[\varphi\star\mathbf{1}](\psi\|\psi), \tag{101}$$

where $\mathbf{1} \in \mathcal{C}_{m\times n}$, $\mathbf{1}_{i,j} = 1$, for all $1 \le i \le m$, $1 \le j \le n$.

Proposition C.6. *If $\phi,\ \psi \in \mathcal{C}_{m\times n}$ are periodic and $\varphi \in \mathcal{V}_{m\times n}$ is even and periodic, then*

$$\left(\phi\middle\|[\varphi\star\psi]\right) = \left(\psi\middle\|[\varphi\star\phi]\right). \tag{102}$$

The proofs of Propositions C.4, C.5, and C.6 can be found in [37]. We remark that these definitions and formulas have straightforward extensions to three dimensions.

Under the assumption that $M(\frac{3}{2}A_x\phi^k - \frac{1}{2}A_x\phi^{k-1})$ and $M(\frac{3}{2}A_y\phi^k - \frac{1}{2}A_y\phi^{k-1})$ are positive, we consider the space

$$H := \{\phi \in C_{m\times n} \mid (\phi\|\mathbf{1}) = 0\}, \tag{103}$$

and equip this space with the bilinear form

$$(\phi_1\|\phi_2)_H := \left[M\left(\frac{3}{2}A_x\phi^k - \frac{1}{2}A_x\phi^{k-1}\right)D_x\psi_1 \middle\| D_x\psi_2\right]_{ew} + \left[M\left(\frac{3}{2}A_y\phi^k - \frac{1}{2}A_y\phi^{k-1}\right)D_y\psi_1 \middle\| D_y\psi_2\right]_{ns} \tag{104}$$

for any ϕ_1, $\phi_2 \in H$, where $\psi_i \in C_{\bar{m}\times\bar{n}}$ is the unique solution to

$$\mathcal{L}(\psi_i) = d_x\left(M\left(\frac{3}{2}A_x\phi^k - \frac{1}{2}A_x\phi^{k-1}\right)D_x\psi_i\right) + d_y\left(M\left(\frac{3}{2}A_y\phi^k - \frac{1}{2}A_y\phi^{k-1}\right)D_y\psi_i\right) = \phi_i, \tag{105}$$

where ψ_i is periodic and $(\psi_i\|\mathbf{1}) = 0$. The proof of the following proposition can be found in [56].

Proposition C.7. *$(\phi_1\|\phi_2)_H$ is an inner product on the space H. Moreover,*

$$(\phi_1\|\phi_2)_H = \left(\phi_1 \middle\| \mathcal{L}^{-1}(\phi_2)\right) = \left(\mathcal{L}^{-1}(\phi_1) \middle\| \phi_2\right). \tag{106}$$

References

[1] N.M. Abukhdeir, D.G. Vlachos, M.S. Katsoulakis, M. Plexousakis, Long-time integration methods for mesoscopic models of pattern-forming systems, J. Comput. Phys. 230 (14) (2011) 5704–5715.
[2] S.M. Allen, J.W. Cahn, A microscopic theory for antiphase boundary motion and its application to antiphase domain coarsening, Acta Mater. 27 (6) (1979) 1085–1095.
[3] A. Almendral, C.W. Oosterlee, Numerical valuation of options with jumps in the underlying, Appl. Numer. Math. 53 (1) (2005) 1–18.
[4] A.J. Archer, Two-dimensional fluid with competing interactions exhibiting microphase separation: theory for bulk and interfacial properties, Phys. Rev. E 78 (3) (2008) 031402.
[5] A.J. Archer, R. Evans, Dynamical density functional theory and its application to spinodal decomposition, J. Chem. Phys. 121 (9) (2004) 4246–4254.
[6] A.J. Archer, M. Rauscher, Dynamical density functional theory for interacting Brownian particles: stochastic or deterministic?, J. Phys. A, Math. Gen. 37 (40) (2004) 9325.
[7] A.J. Archer, M.J. Robbins, U. Thiele, E. Knobloch, Solidification fronts in supercooled liquids: how rapid fronts can lead to disordered glassy solids, Phys. Rev. E 86 (3) (2012) 031603.
[8] N.J. Armstrong, K.J. Painter, J.A. Sherratt, A continuum approach to modelling cell–cell adhesion, J. Theor. Biol. 243 (1) (2006) 98–113.
[9] N.J. Armstrong, K.J. Painter, J.A. Sherratt, Adding adhesion to a chemical signaling model for somite formation, Bull. Math. Biol. 71 (1) (2009) 1–24.
[10] J.W. Barrett, J.F. Blowey, An error bound for the finite element approximation of the Cahn–Hilliard equation with logarithmic free energy, Numer. Math. 72 (1) (1995) 1–20.
[11] J.W. Barrett, J.F. Blowey, H. Garcke, Finite element approximation of the Cahn–Hilliard equation with degenerate mobility, SIAM J. Numer. Anal. 37 (1) (1999) 286–318.
[12] P.W. Bates, On some nonlocal evolution equations arising in materials science, in: Nonlinear Dynamics and Evolution Equations, vol. 48, 2006, pp. 13–52.
[13] P.W. Bates, S. Brown, J. Han, Numerical analysis for a nonlocal Allen–Cahn equation, Int. J. Numer. Anal. Model. 6 (2009) 33–49.
[14] P.W. Bates, J. Han, The Dirichlet boundary problem for a nonlocal Cahn–Hilliard equation, J. Math. Anal. Appl. 311 (1) (2005) 289–312.
[15] P.W. Bates, J. Han, The Neumann boundary problem for a nonlocal Cahn–Hilliard equation, J. Differ. Equ. 212 (2) (2005) 235–277.
[16] P.W. Bates, J. Han, G. Zhao, On a nonlocal phase-field system, J. Nonlinear Anal. 64 (10) (2006) 2251–2278.
[17] J.W. Cahn, On spinodal decomposition, Acta Mater. 9 (9) (1961) 795–801.
[18] J.W. Cahn, J.E. Hilliard, Free energy of a nonuniform system. I. Interfacial free energy, J. Chem. Phys. 28 (2) (2004) 258–267.
[19] A. Chauviere, H. Hatzikirou, I.G. Kevrekidis, J.S. Lowengrub, V. Cristini, Dynamic density functional theory of solid tumor growth: preliminary models, AIP Adv. 2 (1) (2012) 011210.
[20] X. Chen, G. Caginalp, E. Esenturk, Interface conditions for a phase field model with anisotropic and non-local interactions, Arch. Ration. Mech. Anal. 202 (2) (2011) 349–372.
[21] M.A. Choudhary, D. Li, H. Emmerich, H. Löwen, DDFT calibration and investigation of an anisotropic phase-field crystal model, J. Phys. Condens. Matter 23 (26) (2011) 265005.
[22] A. De Masi, E. Orlandi, E. Presutti, L. Triolo, Glauber evolution with Kac potentials. I. Mesoscopic and macroscopic limits, interface dynamics, Nonlinearity 7 (3) (1994) 633.
[23] Q. Du, M. Gunzburger, R.B. Lehoucq, K. Zhou, Application of a nonlocal vector calculus to the analysis of linear peridynamic materials, Technical report 2011-3870J, Sandia National Laboratories, 2011.
[24] Q. Du, M. Gunzburger, R.B. Lehoucq, K. Zhou, Analysis and approximation of nonlocal diffusion problems with volume constraints, SIAM Rev. 54 (4) (2012) 667–696.
[25] K.R. Elder, M. Grant, Modeling elastic and plastic deformations in nonequilibrium processing using phase field crystals, Phys. Rev. E 70 (5) (2004) 51605.
[26] K.R. Elder, M. Katakowski, M. Haataja, M. Grant, Modeling elasticity in crystal growth, Phys. Rev. Lett. 88 (24) (2002) 245701.
[27] R. Evans, The nature of the liquid–vapour interface and other topics in the statistical mechanics of non-uniform, classical fluids, Adv. Phys. 28 (2) (1979) 143–200.
[28] P. Fife, Some nonclassical trends in parabolic and parabolic-like evolutions, in: Trends in Nonlinear Analysis, Springer, 2003, pp. 153–191.
[29] H.B. Frieboes, F. Jin, Y.L. Chuang, S.M. Wise, J.S. Lowengrub, V. Cristini, Three-dimensional multispecies nonlinear tumor growth – II: Tumor invasion and angiogenesis, J. Theor. Biol. 264 (4) (2010) 1254–1278.
[30] H. Gajewski, K. Gärtner, On a nonlocal model of image segmentation, Z. Angew. Math. Phys. 56 (4) (2005) 572–591.
[31] H. Gajewski, K. Zacharias, On a nonlocal phase separation model, J. Math. Anal. Appl. 286 (1) (2003) 11–31.

[32] A. Gerisch, M.A.J. Chaplain, Mathematical modelling of cancer cell invasion of tissue: local and non-local models and the effect of adhesion, J. Theor. Biol. 250 (4) (2008) 684–704.
[33] G. Giacomin, J.L. Lebowitz, Phase segregation dynamics in particle systems with long range interactions I. Macroscopic limits, J. Stat. Phys. 87 (1–2) (1997) 37–61.
[34] G. Giacomin, J.L. Lebowitz, Phase segregation dynamics in particle systems with long range interactions II: Interface motion, SIAM J. Appl. Math. 58 (6) (1998) 1707–1729.
[35] M. Greenwood, N. Provatas, J. Rottler, Free energy functionals for efficient phase field crystal modeling of structural phase transformations, Phys. Rev. Lett. 105 (4) (2010) 045702.
[36] Z. Guan, Numerical analysis of first and second order unconditional energy stable schemes for nonlocal Cahn–Hilliard and Allen–Cahn equations, PhD thesis, University of Tennessee, August 2012.
[37] Z. Guan, C. Wang, S.M. Wise, A convergent convex splitting scheme for the periodic nonlocal Cahn–Hilliard equation, Numer. Math. (2014), http://dx.doi.org/10.1007/s00211-014-0608-2, in press.
[38] T. Hartley, T. Wanner, A semi-implicit spectral method for stochastic nonlocal phase-field models, Discrete Contin. Dyn. Syst., Ser. A 25 (2009) 399–429.
[39] D.J. Horntrop, M.A. Katsoulakis, D.G. Vlachos, Spectral methods for mesoscopic models of pattern formation, J. Comput. Phys. 173 (1) (2001) 364–390.
[40] K.B. Howell, Principles of Fourier Analysis, CRC, 2001.
[41] Z. Hu, S.M. Wise, C. Wang, J.S. Lowengrub, Stable and efficient finite-difference nonlinear-multigrid schemes for the phase field crystal equation, J. Comput. Phys. 228 (15) (2009) 5323–5339.
[42] A. Imperio, L. Reatto, A bidimensional fluid system with competing interactions: spontaneous and induced pattern formation, J. Phys. Condens. Matter 16 (38) (2004) S3769.
[43] A. Imperio, L. Reatto, Microphase separation in two-dimensional systems with competing interactions, J. Chem. Phys. 124 (2006) 164712.
[44] A. Imperio, L. Reatto, Microphase morphology in two-dimensional fluids under lateral confinement, Phys. Rev. E 76 (4) (2007) 040402.
[45] J. Kim, K. Kang, J.S. Lowengrub, Conservative multigrid methods for Cahn–Hilliard fluids, J. Comput. Phys. 193 (2) (2004) 511–543.
[46] C.N. Likos, B.M. Mladek, D. Gottwald, G. Kahl, Why do ultrasoft repulsive particles cluster and crystallize? Analytical results from density-functional theory, J. Chem. Phys. 126 (22) (2007) 224502.
[47] U.M.B. Marconi, P. Tarazona, Dynamic density functional theory of fluids, J. Chem. Phys. 110 (16) (1999) 8032–8044.
[48] R.C. Merton, Option pricing when underlying stock returns are discontinuous, J. Financ. Econ. 3 (1) (1976) 125–144.
[49] N. Pisutha-Arnond, V. Chan, M. Iyer, V. Gavini, K. Thornton, Classical density functional theory and the phase-field crystal method using a rational function to describe the two-body direct correlation function, Phys. Rev. E 87 (1) (2013) 013313.
[50] R.C. Rogers, A nonlocal model for the exchange energy in ferromagnetic materials, J. Integral Equ. Appl. 3 (1) (1991) 85–127.
[51] R.C. Rogers, Some remarks on nonlocal interactions and hysteresis in phase transitions, Contin. Mech. Thermodyn. 8 (1) (1994) 65–73.
[52] E.W. Sachs, A.K. Strauss, Efficient solution of a partial integro-differential equation in finance, Appl. Numer. Math. 58 (11) (2008) 1687–1703.
[53] R.P. Sear, S.W. Chung, G. Markovich, W.M. Gelbart, J.R. Heath, Spontaneous patterning of quantum dots at the air–water interface, Phys. Rev. E 59 (6) (1999) R6255–R6258.
[54] S.M. Wise, Unconditionally stable finite difference, nonlinear multigrid simulation of the Cahn–Hilliard–Hele–Shaw system of equations, J. Sci. Comput. 44 (1) (2010) 38–68.
[55] S.M. Wise, J.S. Lowengrub, H.B. Frieboes, V. Cristini, Three-dimensional multispecies nonlinear tumor growth – I: Model and numerical method, J. Theor. Biol. 253 (3) (2008) 524–543.
[56] S.M. Wise, C. Wang, J.S. Lowengrub, An energy-stable and convergent finite-difference scheme for the phase field crystal equation, SIAM J. Numer. Anal. 47 (3) (2009) 2269–2288.
[57] X. Wu, G.J. van Zwieten, K.G. van der Zee, Stabilized second-order convex splitting schemes for Cahn–Hilliard models with application to diffuse–interface tumor–growth models, Int. J. Numer. Methods Biomed. Eng. 30 (2) (2014) 180–203.
[58] Z. Zhang, Z. Qiao, An adaptive time-stepping strategy for the Cahn–Hilliard equation, Commun. Comput. Phys. 11 (4) (2012) 1261.